Article

Not peer-reviewed version

Modern River-Sand Geochemical Mapping in the Manufahi Municipality and its Surroundings, Timor-Leste: Implications for Provenance

Vital Cruz Malai Araujo Vilanova *, Tomoyuki Ohtani *, Satoru Kojima *, Kazuma Yatabe *, Nene Valente Soares Cristovao *, Aniceta Araujo *

Posted Date: 22 February 2024

doi: 10.20944/preprints202402.1202.v1

Keywords: geochemical mapping; lithological mapping; river sands; principal component analysis; provenance; alteration; silicification; low-grade metamorphism; secondary mineral assemblage.

 doi:10.20944/preprints202402.1202.v1

Article

Modern River-Sand Geochemical Mapping in the Manufahi Municipality and its Surroundings, Timor-Leste: Implications for Provenance

Vital Vilanova [1,2,*], Tomoyuki Ohtani [1,*], Satoru Kojima [1], Kazuma Yatabe [1], Nene Cristovão [2] and Aniceta Araujo [2]

[1] Department of Civil Engineering, Gifu University, 1-1 Yanagido, Gifu 501-1193, Japan
[2] Department of Geology and Petroleum Engineering, National University of Timor Lorosa'e, Hera, Timor – Leste
* Correspondence: araujo.vilanova.vital.cruz.malai.b2@s.gifu-u.ac.jp and ohtani.tomoyuki.g9@f.gifu-u.ac.jp; Tel.: +81-090-9798-7935

Abstract: A regional modern river-sand geochemical mapping study in the majority of the Timor-Leste territory, including the research area, has not been previously reported. This study demonstrated the potential of modern river sand geochemical mapping as an effective method for lithological mapping, particularly in areas that face challenges in conducting efficient geological fieldwork and have limited geological information. A total of 53 modern river sand samples were collected and analyzed. Before examining the samples using wavelength-dispersive X-ray fluorescence for ten major elements, the loss-on-ignition method was employed. In the Clerec drainage basin, SiO_2, CaO, and K_2O showed positive correlations, and CaO was positively correlated with MnO. Similarly, in the Sahe river catchment, a positive relationship was observed between CaO, MnO, and TiO_2. These findings suggested the presence of quartz, manganese, secondary K-bearing minerals, and secondary Ti-bearing minerals in carbonate rocks that have undergone silicification and other alteration processes. The principal component analysis results corroborated the SiO_2/Al_2O_3 and K_2O/Na_2O ratios and the ICV findings. PC1 was related to the variations in Ca–poor and Ca–rich rocks; PC2 indicated notable inputs from SiO_2–rich and SiO_2–poor rocks, and PC3 revealed the possibility of contributions from secondary mineral assemblages related to silicification and low-grade metamorphic processes.

Keywords: geochemical mapping; lithological mapping; river sands; principal component analysis; provenance; alteration; silicification; low-grade metamorphism; secondary mineral assemblage

1. Background and the Purpose of Research

Timor-Leste is a relatively new independent country. It officially gained its independence in 2002. Timor-Leste is located between Southeast Asia and the Pacific region, surrounded by Indonesia's islands, with the western part of the island of Timor shared with Indonesian territory and Australia as its southern neighbor across the Timor Sea (Figure 1A).

Since Portuguese colonization, the geology of Timor-Leste has been studied and mapped. The majority of geological research studies conducted in the territory of Timor-Leste have been concerned with prospecting and discovering oil and natural gas, paleontology, tectonic settings, and stratigraphy [1–26]. However, geochemical mapping studies have not yet been conducted in the majority of the Timor-Leste territory, including the study area.

Timor island is located in a zone where the Australian and the Eurasian plates collide, and it is characterized by active tectonics. This zone has led to the uplifting of land, formation of the landscape, mountain-building processes, installation of overthrust sheets, complex lithological formations, and other geological phenomena and processes within the Timor Island. The terrain of the island is characterized by a rugged topography with steep slopes, large mountains, high peaks, and deep

 doi:10.20944/preprints202402.1202.v1

valleys. External geodynamic processes such as erosion and weathering also contribute to landscape shaping. The lithologic formations installed and deposited on Timor Island are largely composed of non-volcanic strata that range in age from Permian to Quaternary. Tectonically, these formations can be classified into allochthonous, para-autochthonous, and autochthonous units, and are similar to the Asian and Australian successions. Some of these formations have been involved in various geological events and tectonic processes, such as deformation, metamorphism, volcanic activity, mineralization, and hydrothermal alterations, before and after the orogenic phase, which occurred from the Late Jurassic to the Middle Miocene [1–4,8,10,11,18,19,23,25,27–31].

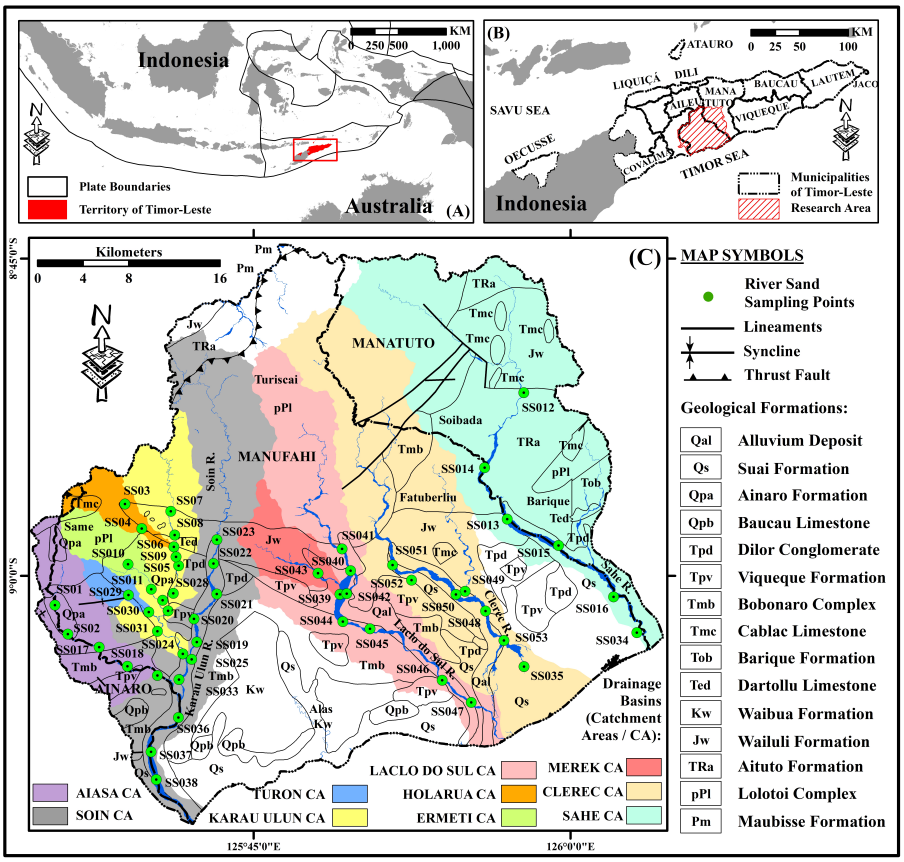

Figure 1. Showing: (**A**) the geographical location of Timor-Leste, (**B**) geographical location of the study area and the surrounding areas, and (**C**) river-sand sampling point distributions with drainage basins and geological formation (adopted from Bachri and Situmorang, 1994; Partoyo et al., 1995) in the study area.

Modern river sands have been used as a sampling medium by numerous researchers in geochemical mapping investigations to determine the relationship between chemical element concentrations and lithological distributions, as well as the location of known or undiscovered mineral deposits [32–43].

Most of the land surface of Timor-Leste, including the study area, is covered by light to dense vegetation as well as deformed, weathered, and erosional geological materials. Direct field geological mapping in these regions may also influence lithological identification capability, especially in characterizing more than one type of source or rock unit [44]. This study demonstrated the potential of river sand geochemical mapping as a lithological mapping tool. Starting with the Manufahi municipality and its surroundings, this study must lead to a future national project establishing a geochemical map of the country that can be utilized for environmental studies, mineral resource discovery, and lithological mapping all over the country. This study aimed to establish a geochemical

 doi:10.20944/preprints202402.1202.v1

database for a limited area of Timor-Leste and to discuss its characteristics and the relationship with the geology of the study area.

2. Geographical and Geological Setting of Timor-Leste and the Study Area

Officially known as Timor-Leste, the eastern portion of Timor encompasses the island of Atauro to the north, the islet of Jaco to the east, and the enclave of Oecusse, which is bordered by Indonesian West Timor, to the west (Figures 1A and 1B).

The study area is located in the municipality of Manufahi and its surroundings on the southern coast of Timor-Leste. The Timor Sea forms the southern border, while Manatuto, Aileu, and Ainaro Municipalities form the eastern, northern, and western borders, respectively (Figure 1B). The study area is a region of rugged mountainous topography with varying slopes, from almost flat to very steep, where it is possible to observe the activities of external geodynamic processes, such as erosion and weathering. The highest elevations are found in the eastern and northern parts of the territory; the highest peak is at Cablac Mountain, with a height of up to 2085 m.

Timor Island, the islet of Jaco, and several other islands in the southeastern region of the Indonesian archipelago are part of the Outer Banda Arc System because of their position in a complex tectonic setting, where two major plates, the Australian and Eurasian plates, collide. Timor Island is characterized by tectonic and geological features, including the predominance of Permian to Cretaceous sedimentary rocks with affinities to Australian and Asian geological sequences that have undergone significant deformation, resulting in complex structures, faulting, and folding. Conversely, Atauro Island, located in the Banda Sea between Timor and Wetar, is linked to the Inner Banda Arc, an area of geological interest due to its volcanic and tectonic characteristics, which are associated with subduction-related processes ([9,13,14,17,45–61]).

Haig et al. (2007 and 2008), and Keep and Haig (2009) have described the five tectonostratigraphic units of Timor Island that are summarized as follows: (**1**) the Gondwana Megasequence is largely composed of allochthonous and para-autochthonous sedimentary rocks from pre-rift sequences that were deposited on the northeastern shelf of the Gondwana continent, and its age ranges from the Permian to the Middle Jurassic; (**2**) the Australian-Margin Megasequence is mostly composed of para-autochthonous sedimentary rocks of the marine environment from post-rift sequences that were deposited on the plateau near the Australian mainland. Its age ranges from the Middle Jurassic to the Middle Miocene, and the initiation of the post-rift sequence deposition at 155 Ma is associated with a significant tectonic event, which is indicated by a break-up unconformity; (**3**) the Banda Terrane units are characterized by Cenozoic igneous rocks and their cover sediments as well as Mesozoic metamorphic basements that are exposed as thrust sheets and emplaced onto Timor-Leste during the collision phase. They are believed to be derived from the Banda Arc and its forearc arc, as well as components of the crustal blocks of Australia; (**4**) the Synorogenic Mélange is primarily composed of a matrix rich in scaly clay that is derived from mudrock-rich pre- and post-rift successions. Tectonic processes have transported and reassembled this sequence into a chaotic mixture; and (**5**) the Synorogenic Megasequence is characterized by autochthonous sedimentary successions installed through uplifting processes and deposited from eroded sediments of existing rocks in the surrounding basin and depressions during the latest Miocene to the Holocene.

The five tectonostratigraphic units are well-preserved from north to south in the study area (Figures 1C and 2), and the contact between these units is a fault and/or unconformity [1–3,15,16,19,20,25,29,45,47,52,62,63]. In the northern to central parts of the study area, the Banda Terrane and its sedimentary cover units were emplaced above the Synorogenic Mélange and Gondwana Megasequences. In the southern part, Synorogenic Megasequences were deposited above the Australian-Margin Megasequences during the latest Miocene to Holocene.

According to Bachri and Situmorang (1994), Partoyo et al. (1995), and the geological research conducted by Audley-Charles (1968) and others [2–4,6–8,10–12,14,15,18–20,22,23,25,28,50,52,53,55,59–61,64–73], the study area consists of the following formations (Figures 1C and 2).

 doi:10.20944/preprints202402.1202.v1

a) Pleistocene–Holocene Suai Formation

It is mostly composed of rudites and arenites, with minor amounts of mud and marls. The particles of the formation were mostly sourced from the Viqueque Formation, Dilor Conglomerate, and Lolotoi Complex. This formation belongs to the Synorogenic Megasequence.

b) Pleistocene–Holocene Ainaro Formation (Ainaro Gravels)

This formation is part of the Synorogenic Megasequence and is primarily composed of matrix-supported conglomerates that are believed to be sediments from an ancient river terrace. Occasionally, calcite lateritic cements fill these sediments, and the irregular surfaces of the river terrace sediments are frequently covered by ferruginous horizons.

c) Lower Pleistocene–Holocene Baucau Limestone (Baucau Formation)

It is predominantly composed of coral reef limestones along with a minor proportion of calcarenites, calcirudites, and conglomerates (submature graywackes). This formation is expected to provide evidence of the uplift of the island. This formation belongs to the Synorogenic Megasequence.

d) Pliocene Dilor Conglomerate (Dilor Formation)

This formation is part of the Synorogenic Megasequence and consists of conglomerates and sandstones with a significant contribution of detritus from the Lolotoi Complex, particularly quartzite.

e) Upper Miocene–Lower Pliocene Viqueque Formation (Synorogenic Viqueque Megasequence)

Lithologically, this formation is separated into lower (described as "more clayey and silty") and upper (characterized as "more silty and sandy") sections. Large amounts of silty marls, marly siltstones, silty claystones, siltstones, and sandstones, along with minor proportions of calcilutites and biocalcarenites are present in the upper section. The lower section is mostly composed of marls, clayey marls, silty marls, claystones, silty claystones, calcilutites, and tuffs, with minor amounts of basal conglomerates and mottled marls. These rocks are mostly formed by foraminifera fossils and skeletal radiolarians as well as rock fragments and mineral particles, which are associated with carbonate, metamorphic, volcanic, and other sedimentary rocks found in the Lolotoi Complex, Maubisse Formation, Aitutu Formation, Wailuli Formation, and Bobonaro Complex. This formation is included in the Synorogenic Megasequence.

f) Middle Miocene Bobonaro Complex (Bobonaro Formation or Bobonaro Scaly-Clay or Bobonaro Mélange or Synorogenic Mélange)

This unit is part of the Synorogenic Mélange and is primarily composed of exotic blocks within a scaly clay matrix. The matrix lithology is similar to that of mudstone of the Wailuli Formation. Exotic blocks of Permian to Cretaceous ages are common and widely distributed, although absent in several areas.

g) Oligocene–Miocene Cablac Limestone (Cablac Formation)

This formation is largely composed of oolitic and peloidal limestones and pelagic carbonates with small amounts of intraformational conglomerates, calcilutites, calcarenites, agglomerates, and tuffaceous rocks. The most common clasts of conglomerates are volcanic rocks, calcilutites containing foraminifera, radiolarian chert, biomicarenites, and detrital minerals, such as quartz and magnetite. Several rocks have been affected by alteration processes such as dolomitization and a few have undergone partial silicification, desilicification, and dedolomitization. This formation belongs to the Banda Terrane unit.

h) Oligocene Barique Formation

This formation belongs to the Banda Terrane unit and is largely composed of mafic to acidic lavas and tuffs, with minor amounts of serpentinites, volcanic conglomerates, and sandstones. Pillow lava is also observed. Significant alterations are observed in most volcanic rocks. Volcanic rocks are considered to have formed at mid-oceanic ridges and volcanic arcs.

 doi:10.20944/preprints202402.1202.v1

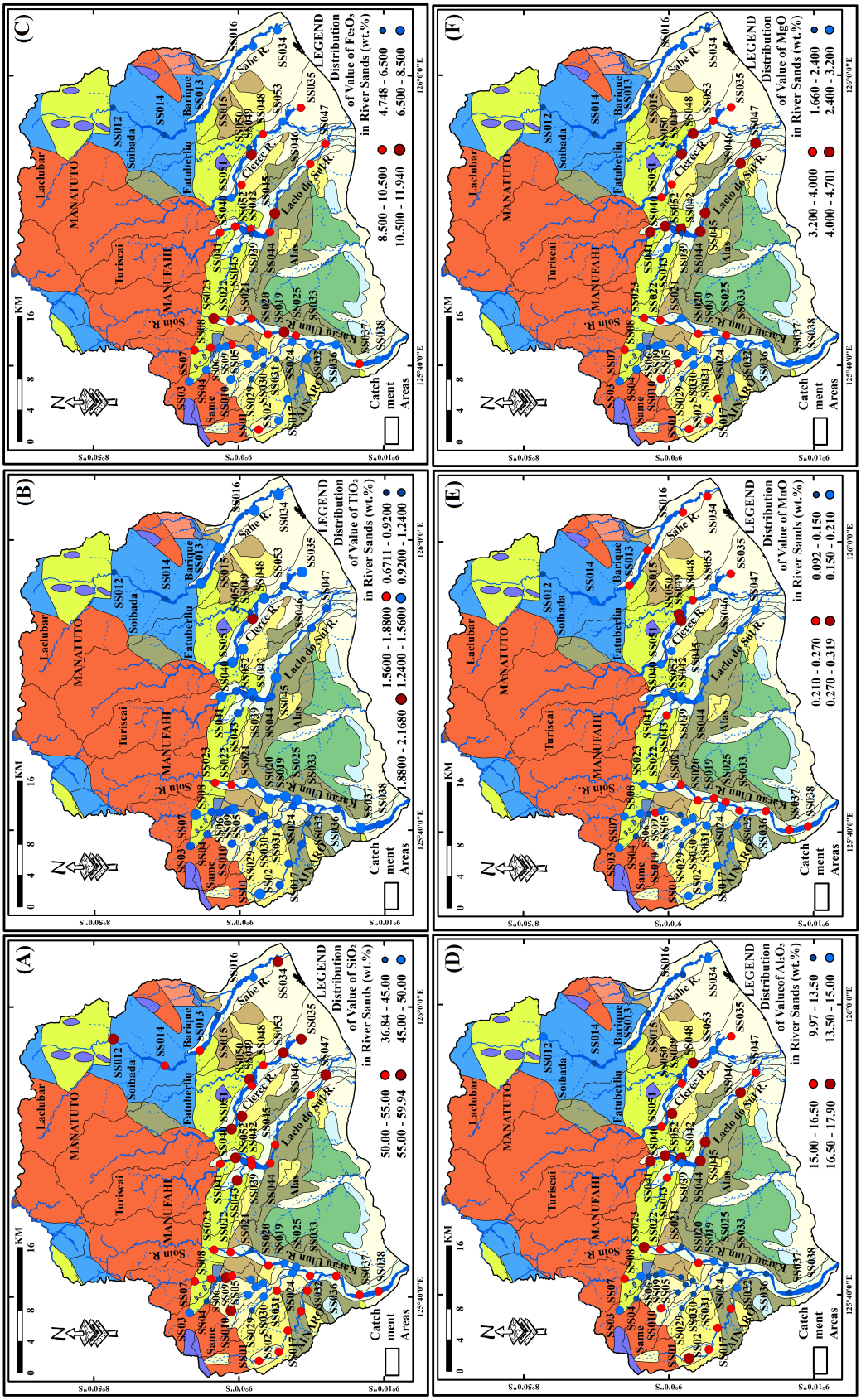

 doi:10.20944/preprints202402.1202.v1

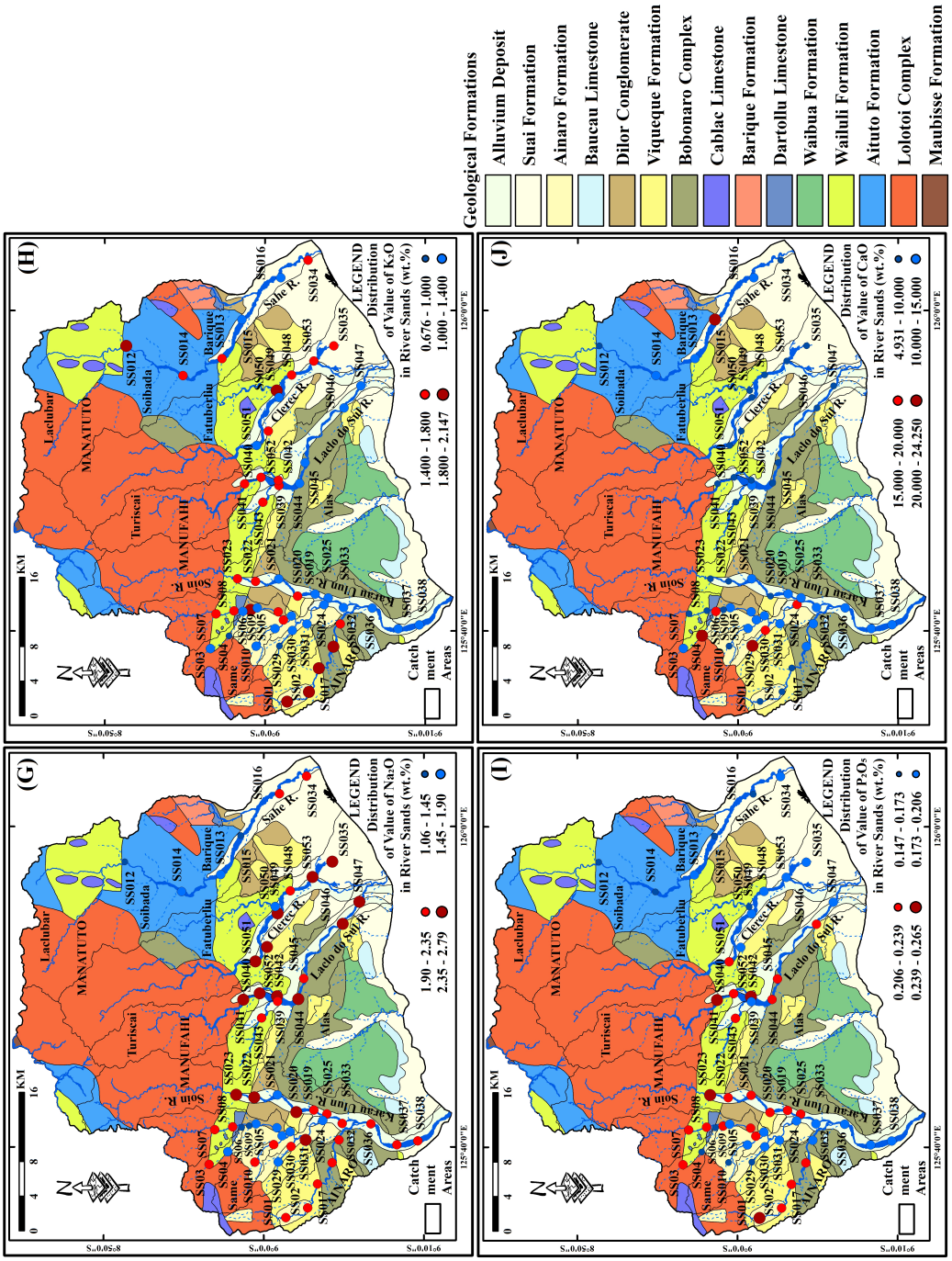

Figure 2. Geological map (adopted from Bachri and Situmorang, 1994; Partoyo et al., 1995) and spatial distribution of major element composition values in the study area. (**A**) SiO_2; (**B**) TiO_2; (**C**) Fe_2O_3; (**D**) Al_2O_3; (**E**) MnO; (**F**) MgO; (**G**) Na_2O; (**H**) K_2O; (**I**) P_2O_5; and (**J**) CaO.

i) Middle–Upper Eocene Dartollu Limestone (Dartolu Formation)

This limestone is part of the Banda Terrane unit and its primary constituents are algal and alveolina biomicarenites with minor proportions of calcilutites, siliceous shales, and siltstones. Dolomitization or silicification was not observed.

j) Lower–Upper Cretaceous Waibua Formation

This formation is part of the Australian-Margin Megasequence and is largely composed of radiolarites, radiolarian cherts, marls, and shales, with several percentages of calcilutites, marls, and calcarenites. Radiolaria and pelagic foraminifera are important components of these rocks

 doi:10.20944/preprints202402.1202.v1

and most limestones are completely or partially silicified. Radiolarian shales, marls, and radiolarites often occur in association with Mn nodules and ferromanganiferous rocks. The formation processes of radiolarites and cherts are closely associated with Mn-rich strata.

k) Late Triassic–Middle Jurassic Wailuli Formation

This formation predominantly consists of gray shales and blue-gray marls with minor amounts of sandstones, mudstones, quartz-arenites, coarse polymictic conglomerates, calcarenites, and calcilutites. Most shales are composed of fine micaceous minerals and microcrystalline carbonates. In some areas, small amounts of pyrite are present in the shales, whereas salt pseudomorphs and gypsum are present in gypsiferous shales, calcilutites, calcarenites, and quartz-arenites. Quartz-arenites contain considerable amounts of mica, and radiolarian and foraminiferal tests are the primary constituents of the calcilutites. This formation is a part of the Gondwana Megasequence.

l) Middle–Upper Triassic Aitutu Formation

This formation consists mostly of calcilutites, shales, and calcareous shales with minor amounts of marls, calcarenites, lumachelles, quartz-arenites, radiolarites, bituminous rocks, and chert. Some calcilutites include radiolarian fragments and the basal part of this formation consists of conglomerates. Radiolarian fossils are significant components of limestones but are partly or almost entirely filled with sparry calcite. Several limestones have been affected by alteration processes such as silicification, dedolomitization, and pyritization. This formation belongs to the Gondwana Megasequence.

m) Triassic–Late Cretaceous Lolotoi Complex (Lolotoi Formation or Lolotoi Metamorphic Complex)

Belonging to the Banda Terrane units, this complex is composed of regionally metamorphosed sedimentary and volcanic rocks, as well as basic and ultrabasic volcanic rocks. These include greenschists, graphitic phyllites, quartz mica schists, amphibolite gneisses and schists, garnet-bearing pelitic gneisses and schists, metagabbros, granulites, garnet mica schists, mafic and felsic igneous, pelitic schists, metabasite schists, carbonate-rich greenschists, peridotites, blueschists, serpentinites, and pyroxenites. The metamorphic rocks of the Lolotoi Complex mostly originate from sedimentary rocks and some metavolcanic rocks have undergone considerable alteration. The forearc region is thought to have been the location of the deposition of sedimentary rocks, and the rock components are thought to have originated from intermediate to mafic continental and oceanic arcs. Volcanic rocks were formed at volcanic arcs and mid-oceanic ridges.

n) Permian–Triassic Maubisse Formation (Maubisse Limestone)

This formation belongs to the Gondwana Megasequence and is mainly composed of fossiliferous limestones and volcanic rocks, as well as other types of sedimentary rocks. These include well-bedded dense biocalcarenites, massive reef limestones, pink crinoidal limestones, calcirudites, sandstones, calcareous shales, micaceous siltstones, tuffs, volcanic conglomerates, basalts, marbles, and metamorphosed basic volcanics. The basalts are pillowed and amygdaloidal and have an alkaline chemical composition. Alteration processes have affected most rocks of the Maubisse Formation, and limestones have been partially affected by alteration processes such as silicification, dolomitization, and chloritization.

3. Sampling and Analytical Methods

3.1. Sampling Method

The sampling methods and sample preparation techniques used in this study were those described by [42,74–78]. A total of 53 modern river sand samples were collected during the dry season from ten permanent rivers or catchment areas (i.e., the Aiasa, Turon, Ermeti, Holarua, Karau Ulun, Soin, Merek, Laclo do Sul, Clerec, and Sahe Rivers) (Figures 1C and 2). Coordinates and other field-related

 doi:10.20944/preprints202402.1202.v1

information, such as geology, geomorphology, and land use, were documented at each sampling point. To avoid sampling errors and heterogeneity of the analytical results, approximately 4 kg of four subsamples were collected over a distance of 20 m at each sampling point. Access conditions, topographic relief, and availability time influenced the sampling point distribution (Figure 3).

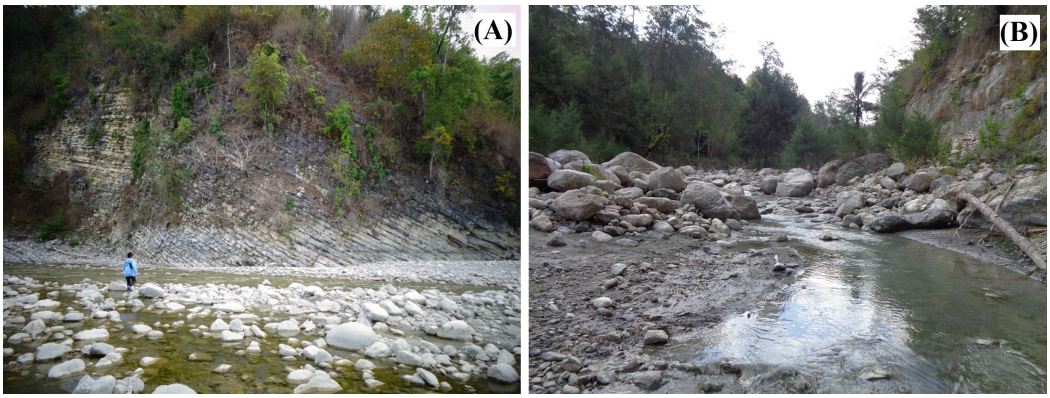

Figure 3. Field photos showing the condition of the sampling points. (**A**) SS014, Sahe River; and (**B**) SS02, Aiasa River.

River sand samples were transported to the laboratory under wet conditions for preparation and chemical analysis. To obtain grain-size fractions of 180–150 μm and <150 μm, the samples were dried in an oven at 105 °C and then sieved using a vibrating sieve shaker machine. Manual crushing using an agate mortar and pestle was followed by machine crushing using a disk mill. Subsequently, the organic matter and volatile substances were removed using the loss-on-ignition method, which was verified by weighing the weight loss after heating at 950 °C.

3.2. Analytical Method

According to Yamamoto and Morishita (1997) [79], glass beads are commonly used for sample preparation in XRF spectrometry analysis. Typically, glass beads are prepared by mixing a flux with a powdered sample.

Glass beads were prepared by fusing mixtures of powdered samples and alkali flux at a weight ratio of 1:10. An 8:2 mixture of lithium tetraborate ($Li_2B_4O_7$) and lithium metaborate ($LiBO_2$) was used as the alkali flux. The mixture was processed to prepare glass beads using a bead sampler machine (TK-4100 model, Amena Tech Co.) after placing the mixed powder in a platinum crucible. At the Division of Instrumental Analysis, Gifu University, modern river sand samples were examined by wavelength-dispersive X-ray fluorescence using a Bruker S8 Tiger with rhodium target X-ray tubes. Ten major elements (SiO_2, TiO_2, Fe_2O_3, Al_2O_3, MnO, MgO, Na_2O, K_2O, P_2O_5, and CaO) were determined and reference samples of igneous and sedimentary rocks provided by the Geological Survey of Japan were used for calibration.

3.3. Statistical Analysis

The major element compositions to be statistically analyzed and discussed were normalized based on the estimated average concentration of elements in the Upper Continental Crust (UCC) [80] and Post-Archean Australian Shale (PAAS) [81] (Table 1, Figure 4).

 doi:10.20944/preprints202402.1202.v1

Table 1. Statistical summary of the major element compositions along with some selected ratios and ICV of the river sand samples from the study area.

Catchment Area		Weight % (wt%)										Ratios		ICV
		SiO_2	TiO_2	Al_2O_3	Fe_2O_3	MnO	MgO	CaO	Na_2O	K_2O	P_2O_5	SiO_2/Al_2O_3	K_2O/Na_2O	
Aiasa	Min.	50.61	0.92	14.10	6.53	0.17	3.12	5.58	2.00	1.64	0.20	2.93	0.80	1.14
	Max.	51.74	1.32	17.60	9.32	0.21	3.67	10.83	2.17	2.15	0.26	3.67	1.04	1.18
	Avg.	51.10	1.09	15.74	7.81	0.18	3.32	9.04	2.07	1.94	0.22	3.26	0.94	1.16
	Std.	0.54	0.15	1.30	1.02	0.02	0.22	2.09	0.06	0.20	0.02	0.27	0.09	0.02
Turon	Min.	39.00	0.67	10.40	4.75	0.09	2.11	16.19	1.57	0.99	0.15	3.75	0.63	1.12
	Max.	47.30	0.88	12.30	5.91	0.15	2.63	24.25	1.96	1.36	0.18	3.85	0.69	1.19
	Avg.	43.15	0.78	11.35	5.33	0.12	2.37	20.22	1.77	1.17	0.17	3.80	0.66	1.15
	Std.	5.87	0.15	1.34	0.82	0.04	0.37	5.70	0.28	0.27	0.02	0.07	0.05	0.05
Ermeti	Min.	47.70	1.08	12.90	7.54	0.14	3.84	6.99	1.95	1.03	0.15	3.50	0.53	1.21
	Max.	55.01	1.14	15.70	8.40	0.18	3.99	14.22	2.09	1.34	0.18	3.70	0.64	1.35
	Avg.	51.36	1.11	14.30	7.97	0.16	3.92	10.61	2.02	1.19	0.16	3.60	0.58	1.28
	Std.	5.17	0.04	1.98	0.61	0.03	0.11	5.11	0.10	0.22	0.02	0.14	0.08	0.10
Holarua	Min.	36.84	1.00	11.00	7.49	0.11	2.27	13.43	1.26	0.68	0.16	3.35	0.41	1.22
	Max.	47.92	1.20	13.80	8.22	0.16	3.12	23.21	2.17	1.28	0.21	3.79	0.86	1.49
	Avg.	43.15	1.10	12.20	7.97	0.14	2.81	18.11	1.69	1.01	0.18	3.54	0.62	1.34
	Std.	5.70	0.10	1.44	0.41	0.03	0.47	4.90	0.46	0.31	0.03	0.23	0.23	0.14
Karau Ulun	Min.	45.52	1.05	12.30	6.41	0.15	2.47	9.56	1.06	1.16	0.18	3.28	0.47	1.16
	Max.	55.50	1.25	15.50	8.94	0.24	3.43	15.99	2.47	1.84	0.23	4.51	1.74	1.32
	Avg.	50.65	1.15	13.49	7.92	0.17	3.00	11.93	1.82	1.40	0.21	3.77	0.83	1.27
	Std.	3.16	0.07	1.02	0.96	0.02	0.28	2.12	0.38	0.21	0.02	0.34	0.36	0.05
Soin	Min.	44.86	1.00	13.20	6.69	0.17	2.88	6.04	1.81	1.27	0.20	3.18	0.59	1.21
	Max.	54.53	1.71	16.60	11.54	0.26	3.61	13.31	2.59	1.64	0.27	4.01	0.77	1.54
	Avg.	51.11	1.39	14.24	9.13	0.22	3.18	10.24	2.27	1.41	0.22	3.61	0.62	1.38
	Std.	3.03	0.21	1.35	1.54	0.03	0.25	2.39	0.24	0.13	0.02	0.32	0.05	0.10
Merek	Min.	53.33	0.78	14.40	6.17	0.19	2.40	6.68	1.92	1.70	0.19	3.70	0.75	1.04
	Max.	58.19	0.94	15.40	7.53	0.26	2.48	10.70	2.26	1.78	0.21	3.78	0.93	1.12
	Avg.	55.76	0.86	14.90	6.85	0.22	2.44	8.69	2.09	1.74	0.20	3.74	0.84	1.08
	Std.	3.44	0.11	0.71	0.96	0.05	0.06	2.84	0.24	0.06	0.01	0.05	0.12	0.05
Laclo do Sul	Min.	50.13	1.14	16.40	8.57	0.16	4.30	4.93	2.28	1.10	0.20	2.93	0.45	1.22
	Max.	55.81	1.50	17.90	11.73	0.19	4.70	7.94	2.74	1.64	0.25	3.37	0.60	1.38
	Avg.	54.11	1.25	17.23	9.55	0.18	4.41	6.21	2.59	1.37	0.23	3.14	0.53	1.26
	Std.	1.86	0.12	0.52	1.00	0.01	0.14	1.14	0.16	0.19	0.02	0.14	0.06	0.05
Clerec	Min.	52.31	0.76	13.10	5.87	0.19	1.66	5.80	1.46	1.24	0.17	3.11	0.50	1.01
	Max.	59.94	2.17	17.00	11.94	0.32	4.41	8.17	2.79	1.88	0.21	4.58	1.29	1.55
	Avg.	56.23	1.38	15.63	8.72	0.24	3.54	6.69	2.37	1.49	0.19	3.63	0.67	1.27
	Std.	2.75	0.44	1.33	1.88	0.05	0.90	0.80	0.44	0.21	0.01	0.48	0.28	0.16
Sahe	Min.	38.30	0.78	9.97	5.99	0.14	1.86	8.20	1.13	1.16	0.15	3.77	0.66	0.93
	Max.	57.20	1.49	14.80	7.51	0.26	2.41	23.49	2.11	2.09	0.19	4.14	1.51	1.35
	Avg.	51.23	1.21	13.08	6.68	0.21	2.16	13.02	1.64	1.53	0.17	3.91	0.97	1.15
	Std.	6.94	0.32	1.63	0.58	0.05	0.20	5.49	0.35	0.34	0.01	0.13	0.32	0.14
-	UCC	66.62	0.64	15.40	5.04	0.10	2.48	3.59	3.27	2.80	0.15	4.33	0.86	1.16
-	PAAS	62.80	1.00	18.90	6.50	0.11	2.20	1.30	1.20	3.70	0.16	3.32	3.08	0.85

Note: Post-Archean Australian Shales (PAAS; Data from Taylor and McLennan, 1985) and upper continental crust (UCC; Data from Rudnick and Gao, 2003) values are also presented for comparison. ICV = index of compositional variability; Min. = minimum; Max.= maximum; Avg. = average; and Std. = standard deviation.

 doi:10.20944/preprints202402.1202.v1

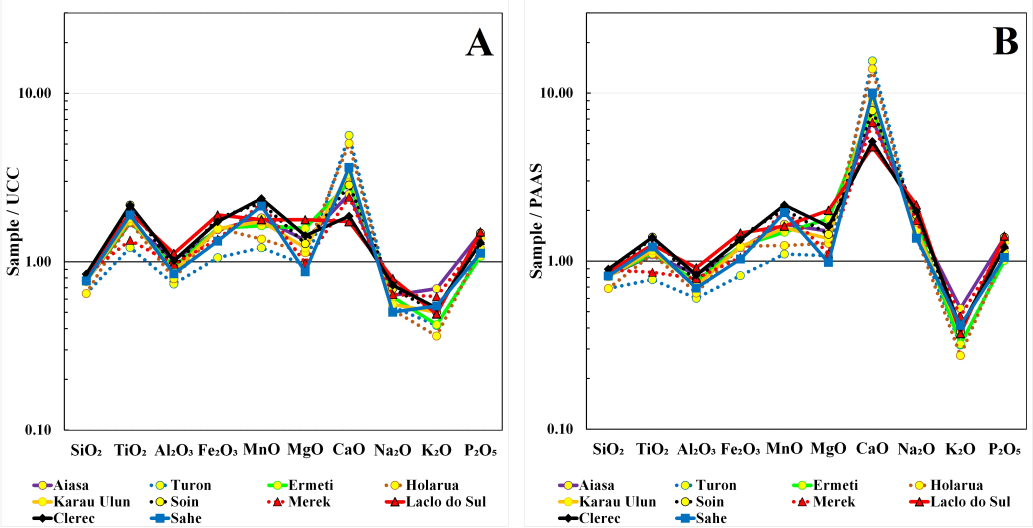

Figure 4. Spider plots of the major element compositions. They are normalized using (**A**) the upper continental crust (UCC; Data from Rudnick and Gao, 2003) and (**B**) Post-Archaean Australian Shale (PAAS; Data from Taylor and McLennan, 1985).

To simplify and evaluate the results of the geochemical analysis by reducing the dimensionality of the datasets, exploring elemental associations, and allowing the interpretation of variance within the dataset based on major controlling factors, a multivariate statistical technique, principal component analysis (PCA), was used. To analyze and interpret PCA results in a biplot of joint graphical representations of variables and samples, only principal components with eigenvalues greater than or near 1.0 were used because they explain the majority of the variance in the data [82,83].

In this study, several ratios of selected major elements, the Pearson correlation coefficient matrix, and the index of compositional variability (ICV) were used to analyze and interpret provenance [32,35,40,84–89].

The ICV was calculated as weight percent (wt%) proportions (ICV = $[Fe_2O_3 + K_2O + Na_2O + CaO^* + MgO + MnO + TiO_2]/Al_2O_3$) [90]. To avoid mistakes in the analysis and interpretation of ICV values due to carbonate materials, which are abundant in the majority of sediments and sedimentary rocks [91], as well as the carbonate rocks that contribute to the CaO enrichment in river sand samples, the CaO^* value represents Ca, which is only present in silicate minerals. According to the concept that the molecular CaO/Na_2O ratio of silicate is not greater than one, the CaO^* value is considered to be equivalent to the Na_2O content [22,92].

Chemical and statistical analyses were performed using Microsoft Office Excel and JMP Pro 14.0. A geographical map was created using ArcGIS 10.4.

4. Analytical Results

4.1. Geochemical Features of River Sand Samples

Chemical analyses of river sand samples from the ten drainage basins in the study area revealed that the major oxides with the highest concentrations in the samples were SiO_2 (ranging from 36.84 to 59.94 wt%), CaO (ranging from 4.93 to 24.25 wt%), and Al_2O_3 (ranging from 9.97 to 17.90 wt%). Meanwhile, TiO_2, Fe_2O_3, MnO, MgO, Na_2O, K_2O, and P_2O_5 contents ranged from 0.67 to 2.17, 4.75 to 11.94, 0.09 to 0.32, 1.66 to 4.70, 1.06 to 2.79, 0.68 to 2.15, and 0.15 to 0.27 wt%, respectively.

The evaluation results on the statistical summary (Table 1) and spatial distributions of major element concentration values in the study area (Figure 2) indicated that the drainage basins occupied by the Wailuli Formation were rich in SiO_2 (55.81–59.94 wt%), TiO_2 (1.60–2.17 wt%), Al_2O_3 (16.60–17.90 wt%), Fe_2O_3 (11.54–11.94 wt%), MnO (0.25–0.32 wt%), Na_2O (2.48–2.74 wt%), K_2O (1.88–2.09 wt%),

 doi:10.20944/preprints202402.1202.v1

and P_2O_5 (0.25–0.27 wt%). These areas also mostly exhibited low CaO concentrations (ranging from 4.93 to 8.20 wt%).

The drainage basins occupied by the Viqueque Formation also had high concentrations of Na_2O, K_2O, SiO_2, Al_2O_3, and MgO, whereas the basins covered by the Dilor Conglomerate were abundant in P_2O_5, Fe_2O_3, MnO, and TiO_2. The highest concentrations of CaO were recorded near the midstream areas of the Sahe and Turon River catchments, which were covered by the Aitutu and Viqueque Formations, whereas the other major elements mostly showed the lowest measured contents. In the midstream area of the Holarua River catchment (SS04, near the contact between the Lolotoi Complex, Wailuli Formation, and Ainaro Formation), abundant concentrations of CaO and the lowest reported contents of all other major elements were also observed.

The areas near the midstream of the Laclo do Sul River Basin, specifically those occupied by the Bobonaro Complex, where the highest MgO values were identified, also showed higher concentrations of Al_2O_3, Fe_2O_3, MnO, and Na_2O. High concentrations of K_2O, SiO_2, Al_2O_3, MgO, Na_2O, and P_2O_5 were also found in nearby areas of the Aiasa River catchment upstream, Karau Ulun River catchment downstream, and Ermeti River catchment, particularly those occupied by the Ainaro Formation. In addition, the downstream areas of the Karau Ulun, Laclo do Sul, Clerec, and Sahe River catchments, which were occupied by the Suai Formation, were also abundant in SiO_2, MnO, Na_2O, Fe_2O_3, MgO, and K_2O.

4.2. Comparison with UCC and PAAS

The results of the UCC- and PAAS-normalized patterns for the major elements of the river sand samples from the study area are shown in Figure 4. The bulk composition of the UCC is granodioritic and representative of the continental crust [80]. In contrast, PAAS represents a crustal shale sedimentary rock bulk composition [81].

In comparison with the average major element compositions of the UCC and PAAS (Figures 4A and 4B), the composition of the river sand samples from the ten drainage basins revealed a significant depletion in K_2O, a slight depletion in SiO_2, a slight depletion to considerable enrichment in MgO, a slight enrichment in P_2O_5, slight to considerable enrichments in TiO_2, Fe_2O_3, and MnO, and considerable to significant enrichments in CaO. However, Turon and Holarua had more abundance and Laclo do Sul and Clerec had lower abundance than in the other river catchments. The UCC-normalized patterns (Figure 4A) showed considerable depletion of Na_2O, and the concentration of Al_2O_3 was enriched in the Aiasa, Laclo do Sul, and Clerec drainage basins and depleted in the other river catchments. In contrast, compared to the average composition of the PAAS (Figure 4B), Na_2O was enriched and Al_2O_3 was depleted.

The abundance of CaO, depletion of K_2O, and variations in Na_2O concentrations were mostly controlled by the destruction of carbonate, clay and plagioclase minerals, which contributed to the river sand sample compositions from the study area. The enrichment of TiO_2, Fe_2O_3, MnO, P_2O_5, and MgO could be related to the contribution of mafic, heavy, and accessory minerals (such as amphibole, pyroxene, biotite, ilmenite, hematite, sphene, rutile, garnet, and other minerals) as well as manganese and phosphate minerals. The depletion of SiO_2 and Al_2O_3 concentrations also supports the findings that the majority of the rocks in the study area were calcareous cover sediments at the northern edge of the Australian continental shelf. Sedimentary and metamorphic rocks rich in mafic components were also present.

4.3. Geochemical Characteristics of Some Drainage Basins

The results of the Pearson correlation coefficient matrix for the major element compositions of river sand samples from the selected catchment areas (Tables 2A-D) and the spatial distribution of major element contents in the study area (Figure 2) are as follows:

1) Soin River catchment

 doi:10.20944/preprints202402.1202.v1

As shown in Table 2A, SiO_2 showed a positive correlation with Al_2O_3, MgO, Na_2O, and K_2O, as opposed to Al_2O_3, which was negatively associated with MnO and CaO and positively correlated with all other major elements. CaO had a strong positive association with MnO and a negative relationship with all other elements. Positive relationships were observed between TiO_2, Fe_2O_3, MgO, Na_2O, K_2O, and P_2O_5. These findings suggest that silicate, heavy, and accessory minerals (such as quartz, plagioclases, amphiboles, ilmenites, rutiles, garnets, apatites, sphenes, muscovites, and chlorites) as well as calcium carbonate, manganese, mica, and clay minerals contributed to the composition of river sand samples in this river catchment.

The highest observed amounts of TiO_2, Al_2O_3, MgO, Na_2O, K_2O, P_2O_5, Fe_2O_3, and SiO_2, along with the lowest measured concentrations of CaO and MnO, were mostly recorded near the upstream areas. The midstream regions had the lowest observed SiO_2 content and the highest measured concentrations of CaO, MnO, and Fe_2O_3. In addition, the downstream regions had the highest SiO_2 content, high concentrations of CaO and MnO, and low concentrations of P_2O_5, MgO, TiO_2, Fe_2O_3, and Al_2O_3. This indicated that the upstream areas were mostly influenced by clay and mica content as well as quartz, plagioclase, amphibole, chlorite, hematite, ilmenite, rutile, garnet, sphene, and apatite minerals, which are associated with siliciclastic sedimentary and metamorphic rocks. Carbonate components and Mn minerals affiliated with calcareous sedimentary rocks, along with the clay content associated with shales and mudstones, made major contributions to the midstream regions. The downstream regions were mostly controlled by silicate minerals, such as quartz associated with siliceous sedimentary rocks, carbonate components, and manganese minerals affiliated with carbonaceous sedimentary rocks, along with clay content related to shales and mudstones.

2) Laclo do Sul River catchment

As shown in Table 2B, SiO_2 was positively correlated with Na_2O, K_2O, P_2O_5, and Al_2O_3. Al_2O_3 was positively associated with SiO_2, TiO_2, Fe_2O_3, Na_2O, K_2O, and P_2O_5. Moderate-to-very strong correlations were observed between TiO_2, Fe_2O_3, MnO, MgO, and CaO. These results suggested the major contributions of clay and mica minerals, along with silicate, heavy, and accessory minerals (such as quartz, plagioclase, feldspar, amphibole, pyroxene, biotite, ilmenite, hematite, sphene, rutile, and garnet), which significantly contributed to the geochemical composition of the river sand samples from this river catchment.

The Al_2O_3 concentration appeared to increase in the upstream direction. High SiO_2, Al_2O_3, K_2O, P_2O_5, Na_2O, TiO_2, Fe_2O_3, and MgO contents and low CaO and MnO concentrations were recorded near the upstream areas. Downstream and midstream regions, specifically sample location SS045, had high concentrations of Fe_2O_3, MgO, TiO_2, and MnO and low Na_2O and K_2O contents. In addition, high values of SiO_2, Na_2O, and CaO, along with low concentrations of TiO_2, Fe_2O_3, and Al_2O_3, were also observed in the downstream area. The destruction of clay and mica, along with quartz, plagioclase, amphibole, chlorite, hematite, ilmenite, rutile, garnet, sphene, and apatite minerals associated with siliciclastic sedimentary and metamorphic rocks, contributed significantly to the composition of the river sands near the upstream regions. Near the downstream and continuing to the midstream regions, quartz and clay contents affiliated with shales and mudstones made major contributions; however, there were significant inputs from mafic and heavy minerals associated with igneous and metamorphic rocks at sample location SS045. Silicate minerals and clay related to sedimentary rocks contributed significantly to the downstream area.

3) Clerec River catchment

As demonstrated by the Pearson correlation of the Clerec River catchment (Table 2C), SiO_2 showed a positive association with CaO and TiO_2, Al_2O_3 had a positive correlation with TiO_2, Fe_2O_3, Na_2O, P_2O_5, and MgO, and CaO showed a positive correlation with SiO_2, MnO, and K_2O. There was a moderate-to-very strong positive relationship between TiO_2, Fe_2O_3, MgO, Na_2O, and P_2O_5, indicating that the destruction of clay, mica, amphibole, pyroxene, biotite, ilmenite,

 doi:10.20944/preprints202402.1202.v1

hematite, sphene, rutile, garnet, and apatite, along with calcium carbonate, manganese, and alteration minerals, contributed significantly to the composition of the river sand from this river catchment. The positive correlations between SiO_2, CaO, and K_2O indicated that they may have been derived from the same source. The elevated K_2O level may be related to the presence of secondary K-bearing minerals.

The CaO content tended to increase downstream; however, the highest measured concentration in this river catchment was recorded at the sample site SS049. In the midstream regions, high contents of Al_2O_3, Na_2O, and P_2O_5 and the lowest concentrations of CaO and MnO were recorded. The reported distribution of the elemental concentrations near the downstream regions showed high measured values of TiO_2, Al_2O_3, Fe_2O_3, MgO, MnO, and P_2O_5. In contrast, elevated values of SiO_2, K_2O, and MnO were recorded at sample site SS049. The downstream regions also appeared to have high concentrations of SiO_2, Na_2O, and Al_2O_3 and low TiO_2 and CaO contents. These findings suggest that the midstream areas were largely influenced by quartz, clay, and mica contents as well as lithic fragments, which are associated with siliciclastic sedimentary rocks. Near the downstream regions, clay, muscovite, quartz, plagioclase, chlorite, sphene, garnet and apatite minerals affiliated with siliciclastic sedimentary rocks and their altered rocks owing to metamorphic processes made major contributions. However, sample location SS049 was characterized by notable inputs from quartz, calcium carbonate, manganese, and secondary K-bearing minerals, which were associated with altered carbonate rocks intercalated with shales due to silicification processes. In addition, there were major contributions from silicate and clay contents related to sedimentary rocks in the downstream areas.

Table 2. Correlation coefficient matrix (Pearson) between major element compositions of the river sand samples from each river catchment in the study area. (**A**) Soin; (**B**) Laclo do Sul; (**C**) Clerec; and (**D**) Sahe.

SOIN	SiO_2	TiO_2	Al_2O_3	Fe_2O_3	MnO	MgO	CaO	Na_2O	K_2O	P_2O_5	SiO_2/Al_2O_3
SiO_2	**1.00**										
TiO_2	-0.26	**1.00**									
Al_2O_3	0.36	0.71	**1.00**								
Fe_2O_3	-0.43	0.93	0.59	**1.00**							
MnO	-0.60	-0.32	-0.76	-0.20	**1.00**						
MgO	0.10	0.90	0.92	0.75	-0.63	**1.00**					
CaO	-0.60	-0.57	-0.94	-0.43	0.81	-0.81	**1.00**				
Na_2O	0.68	0.45	0.87	0.25	-0.78	0.73	-0.91	**1.00**			
K_2O	0.27	0.60	0.94	0.56	-0.74	0.80	-0.85	0.77	**1.00**		
P_2O_5	-0.20	0.91	0.79	0.90	-0.43	0.88	-0.60	0.53	0.74	**1.00**	
SiO_2/Al_2O_3	0.33	-0.90	-0.76	-0.89	0.33	-0.86	0.53	-0.41	-0.77	-0.94	**1.00**

LACLO DO SUL	SiO_2	TiO_2	Al_2O_3	Fe_2O_3	MnO	MgO	CaO	Na_2O	K_2O	P_2O_5	SiO_2/Al_2O_3
SiO_2	**1.00**										
TiO_2	-0.96	**1.00**									
Al_2O_3	0.11	0.14	**1.00**								
Fe_2O_3	-0.95	0.99	0.12	**1.00**							
MnO	-0.77	0.64	-0.31	0.69	**1.00**						
MgO	-0.94	0.90	-0.15	0.90	0.77	**1.00**					
CaO	-0.67	0.48	-0.76	0.51	0.77	0.66	**1.00**				
Na_2O	0.96	-0.89	0.18	-0.90	-0.86	-0.87	-0.75	**1.00**			
K_2O	0.66	-0.46	0.73	-0.44	-0.73	-0.71	-0.92	0.70	**1.00**		
P_2O_5	0.15	0.04	0.87	-0.02	-0.45	-0.29	-0.80	0.23	0.74	**1.00**	
SiO_2/Al_2O_3	0.71	-0.86	-0.61	-0.84	-0.39	-0.64	0.00	0.64	0.01	-0.49	**1.00**

CLEREC	SiO_2	TiO_2	Al_2O_3	Fe_2O_3	MnO	MgO	CaO	Na_2O	K_2O	P_2O_5	SiO_2/Al_2O_3
SiO_2	**1.00**										
TiO_2	-0.90	**1.00**									
Al_2O_3	-0.61	0.58	**1.00**								
Fe_2O_3	-0.94	0.99	0.63	**1.00**							
MnO	-0.11	0.05	-0.58	0.02	**1.00**						
MgO	-0.78	0.74	0.94	0.79	-0.52	**1.00**					
CaO	0.21	-0.28	-0.82	-0.32	0.91	-0.77	**1.00**				
Na_2O	-0.33	0.50	0.78	0.50	-0.82	0.80	-0.93	**1.00**			
K_2O	0.51	-0.76	-0.57	-0.73	0.49	-0.72	0.64	-0.87	**1.00**		
P_2O_5	-0.65	0.66	0.91	0.70	-0.47	0.90	-0.79	0.75	-0.61	**1.00**	
SiO_2/Al_2O_3	0.82	-0.78	-0.95	-0.83	0.41	-0.99	0.70	-0.73	0.66	-0.90	**1.00**

SAHE	SiO_2	TiO_2	Al_2O_3	Fe_2O_3	MnO	MgO	CaO	Na_2O	K_2O	P_2O_5	SiO_2/Al_2O_3
SiO_2	**1.00**										
TiO_2	-0.39	**1.00**									
Al_2O_3	0.97	-0.46	**1.00**								
Fe_2O_3	0.03	0.88	-0.03	**1.00**							
MnO	-0.46	0.99	-0.51	0.86	**1.00**						
MgO	0.53	0.30	0.52	0.52	0.29	**1.00**					
CaO	-0.99	0.41	-0.99	-0.02	0.47	-0.53	**1.00**				
Na_2O	0.62	0.26	0.53	0.47	0.22	0.95	-0.58	**1.00**			
K_2O	0.67	-0.83	0.73	-0.51	-0.86	-0.19	-0.70	-0.15	**1.00**		
P_2O_5	0.38	0.60	0.24	0.75	0.56	0.81	-0.33	0.89	-0.40	**1.00**	
SiO_2/Al_2O_3	0.47	0.11	0.23	0.20	0.00	0.22	-0.38	0.52	0.03	0.61	**1.00**

4) Sahe River catchment

CaO had a positive correlation with TiO_2 and MnO and SiO_2 showed a very strong association with Al_2O_3 and they had a moderate-to-strong positive relationship with MgO, Na_2O, and K_2O (Table 2D). Positive associations were observed between TiO_2, Fe_2O_3, MnO, MgO, Na_2O, and P_2O_5. These findings indicated that there were inputs of calcium carbonate, clay, muscovite, manganese, quartz, plagioclase, feldspar, amphibole, biotite, chlorite, ilmenite, hematite, rutile, garnet, sphene, and apatite. The presence of TiO_2 in carbonate rocks associated with Mn minerals

 doi:10.20944/preprints202402.1202.v1

is not common. TiO_2 could be associated with Mn minerals in carbonate rocks, suggesting the presence of secondary Ti-bearing minerals owing to certain alteration processes.

In this river catchment, the highest concentrations of SiO_2 and K_2O appeared in areas near the upstream regions, along with the lowest concentrations of TiO_2, Fe_2O_3, Na_2O, MnO, and CaO. Although high measured concentrations of SiO_2, K_2O, and MnO were reported in the midstream regions, sample location SS015 also appeared to have high measured contents of CaO and MnO and low concentrations of SiO_2, Al_2O_3, K_2O, and Na_2O. The downstream regions were also reported to have high SiO_2, Na_2O, K_2O, MgO, and MnO contents. This indicate that the composition of the river sand sample near the upstream area and sample location SS013 was mostly controlled by the destruction of quartz, clay, and mica minerals, which were affiliated with siliciclastic sedimentary rocks; however, silicate and accessory minerals (such as quartz, muscovite and garnet minerals), which are associated with their altered rocks due to metamorphic processes, contributed to the sample location SS013. Sample sites SS014 and SS015 had contributions from calcium-carbonate minerals associated with carbonate rocks; however, there were notable inputs from quartz and secondary K-bearing minerals affiliated with altered carbonate rocks intercalated with shales strata due to silicification processes in the sample location SS014, and considerable contributions to SS015 came from calcium carbonate, manganese, and Ti-bearing minerals, which were also associated with altered carbonate rocks intercalated with shales strata due to certain alteration processes. The downstream regions were characterized by contributions from quartz, clay, carbonate, mica, amphibole, chlorite, ilmenite, garnet, and other minerals related to sedimentary rocks.

5. Discussion

5.1. Relationship between River Sand Geochemistry and Provenance Geology

The SiO_2/Al_2O_3 and K_2O/Na_2O ratios, as well as the geochemical index of ICV, are also frequently used to evaluate the abundance of quartz, clay, K-feldspar, plagioclase, and other less resistant minerals to identify provenance [32,35,40,84–90,93–95]. The SiO_2/Al_2O_3 ratio has different average values for determining source rock compositions and sediment maturities in clastic sediments; in basic igneous rocks, the ratio is approximately 3 and the ratio is approximately 5 in acidic igneous rocks. Hereafter, in clastic sediments, values >5 indicate compositionally mature sediments and values >10 indicate high maturity and potential recycling [86,88,89,95,96].

In the study area, the values of SiO_2/Al_2O_3 ratios ranged from 2.93 to 4.58, with an average of 3.59, slightly higher than PAAS but slightly lower than UCC (Table 1), suggesting that river sand compositions were not as silica and aluminum-rich as the average composition of typical crustal shale and granodiorite. Most of the selected drainage basins showed negative associations between the SiO_2/Al_2O_3 ratios and elements such as TiO_2, MgO, Fe_2O_3, Na_2O, and P_2O_5 (Table 2A-D), suggesting that these elements were not highly associated with silicate minerals but were incorporated into clay minerals. These results indicated that the river sand composition in the study area was largely derived from crustal carbonate sources. In the study area, the major contributions of carbonate components were mostly attributed to the presence of calcareous sedimentary rocks, such as calcilutites, calcareous shales, and marls. These rocks are mainly associated with the Aitutu, Wailuli, and Viqueque Formations.

The K_2O/Na_2O ratio also has variational values in defining the abundance of K-feldspar relative to plagioclase; with high values (> 1) suggesting potential contributions from alkali feldspar or mica and/or possibly from secondary K-bearing minerals, whereas for the abundance of sodium-bearing minerals or plagioclase, the ratios were < 1 [84,87–89].

The K_2O/Na_2O ratios in the study area ranged from 0.41 to 1.74, with an average of 0.73, which was much lower than those of UCC and PAAS (Table 1). Compared with the UCC, the K_2O and Na_2O concentrations showed greater depletion, which could be related to the low contribution of

 doi:10.20944/preprints202402.1202.v1

feldspathic minerals [88,97,98]. These results indicated that the river sand content in the study area was also characterized by an abundance of aluminosilicate compared to feldspar. The highest values of the K_2O/Na_2O ratio (>1) were identified at several sampling points (Figure 5), which were mostly characterized by notable inputs from aluminosilicate and accessory minerals such as clays and muscovites. These minerals were mainly sourced from claystones, siltstones, sandstones, mica schist, and other metamorphic rocks rich in accessory minerals, such as muscovites, as well as shales, micaceous shales, micaceous sandstones, and their altered forms owing to metamorphic processes, which were affiliated with the Viqueque Formation, Dilor Conglomerate, and Wailuli Formation, respectively. However, sample locations SS049, SS014, and SS015 revealed features indicative of the presence of secondary K-bearing minerals associated with altered carbonate rocks intercalated with shales, as a result of silicification and certain alteration processes. These altered rocks are associated with the Aitutu and Wailuli Formations.

Cox et al. (1995) also determined ICV values greater than 1 for the sediments rich in non-clay minerals (chlorites, feldspars, amphiboles, and pyroxenes), whereas values less than 1 were found for sediments with significant concentrations of clay minerals (kaolinite, illite and montmorillonite) [32,84,86,88,89].

The ICV values in the study area ranged from 0.93 to 1.55, with an average of 1.26, which was much higher than those of PAAS and UCC (Table 1). The high concentrations of TiO_2, Fe_2O_3, MnO, MgO, and P_2O_5 compared with UCC and PAAS, as well as the positive association between these elements in most drainage basins, corroborate the presence of mafic sources containing heavy and accessory minerals (such as amphibole, pyroxene, biotite, ilmenite, hematite, sphene, rutile, and garnet) [84,99]. These results revealed the abundance of chlorite minerals along with mafic, heavy, and accessory minerals in the river sand. The occurrence of basic igneous and metamorphic rocks is mainly responsible for the contribution of these minerals to the research area. These rocks are affiliated with the Lolotoi Complex; however, they can be integrated into sedimentary rock fragments and matrices associated with the Aitutu, Wailuli, and Viqueque Formations and/or incorporated into mudstones and shales within the Bobonaro Complex as exotic blocks.

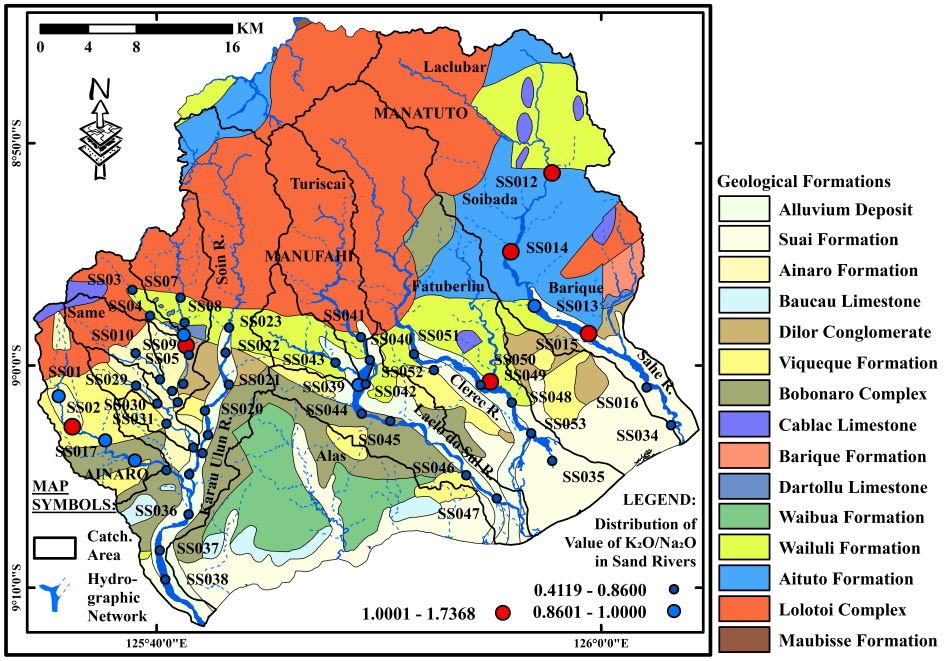

Figure 5. Geological map (adopted from Bachri and Situmorang, 1994; Partoyo et al., 1995) and spatial distribution of K_2O/Na_2O ratio in the study area.

 doi:10.20944/preprints202402.1202.v1

5.2. PCA

PCA was conducted on the major elemental compositions of stream sediments from the ten river catchments in the study area to determine their provenance. The first three principal components of the samples and variables with eigenvalues greater than or near 1.0 were processed for analysis and interpretation (Figure 6) [82,83].

The PCA results for the variables and samples are presented in Tables 3 and 4 and in Figures 7 and 8. The first, second, and third principal components accounted for approximately 49.74%, 20.23%, and 13.61% of the total explanations, respectively.

As shown in Tables 3 and 4 and Figures 7 and 8, PC1 had a strong negative association with *CaO* (-0.40), especially for samples SS029 (-6.23), SS015 (-5.05), SS04 (-4.22), SS06 (-4.00), SS030 (-2.84), and SS014 (-2.55). Negative PC1 scores were attributed to the inputs from Ca-rich rocks. As the carbonate minerals were solely composed of *CaO*, it can be concluded that the carbonate components contributed more to the negative values of PC1. The abundance of carbonate components may be related to the presence of calcilutites, calcareous shales, marls, and conglomerates rich in carbonate rock fragments in the Aitutu, Wailuli, Viqueque, and Ainaro Formations. PC1 had a strong positive correlation with Al_2O_3 (0.42), Na_2O (0.37), MgO (0.36), Fe_2O_3 (0.35), and P_2O_5 (0.33) for the samples SS023 (3.56), SS050 (3.24), SS040 (3.20), SS041 (3.14), SS042 (3.11), and SS01 (2.81). Ca-poor rocks were correlated with positive PC1 values. These samples were collected from shale-, claystone-, siltstone-, marl-, and mudstone-rich formations, which are associated with the Wailuli, Viqueque, Suai, and Ainaro Formations and the Bobonaro Complex. Clay minerals rich in Al_2O_3, Na_2O, MgO, Fe_2O_3, and P_2O_5 in the shales, claystones, siltstones, marls, and mudstones of these formations were highly positively correlated with PC1.

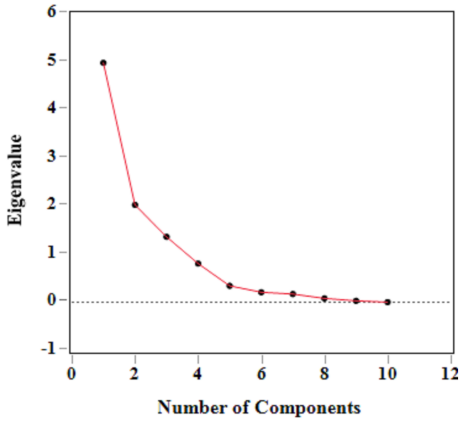

Figure 6. A scree plot showing eigenvalues of each principal component.

Table 3. The first four principal components of the variables with eigenvalues greater than or near 1.0

	PC1	PC2	PC3
Eigenvalues	**4.97**	**2.02**	**1.36**
Explanation (%)	**49.74**	**20.23**	**13.61**
SiO_2	0.2759	-0.4652	0.0452
TiO_2	0.2586	0.4009	0.4187
Al_2O_3	0.4157	-0.1197	-0.2033
Fe_2O_3	0.3452	0.3725	0.1116
MnO	0.1122	-0.0577	0.7712
MgO	0.3553	0.2546	-0.3164
CaO	-0.4014	0.2846	0.0061
Na_2O	0.3666	0.0892	-0.2309
K_2O	0.1390	-0.5558	0.1306
P_2O_5	0.3336	0.0618	0.0602

 doi:10.20944/preprints202402.1202.v1

PC2 was strongly and positively associated with TiO_2 (0.40), Fe_2O_3 (0.37), CaO (0.28), and MgO (0.25), particularly in the following samples: SS04 (3.64), SS050 (2.64), SS045 (2.35), SS015 (2.06), SS019 (1.60), and SS025 (1.58). Input from SiO_2-poor rocks may explain the positive values of PC2. The elemental association of the positive values of PC2, possibly related to the contributions from mafic, heavy, and accessory mineral (such as amphiboles, pyroxenes, biotites, ilmenites, hematites, titanites, rutile, garnet, apatite, and others) inputs, is mainly attributed to the occurrence of basic igneous and metamorphic rocks in the study area. These rocks are associated with the Lolotoi Complex, but they may also be integrated into sedimentary rock fragments and matrices associated with the Aitutu, Wailuli, Viqueque, Ainaro, and Suai Formations as well as the Dilor Conglomerate. These rocks may have also been incorporated into mudstones and shales as exotic blocks within the Bobonaro Complex. Component 2 also had strong negative loadings for K_2O (-0.56) and SiO_2 (-0.47). Negative PC2 scores were observed for samples SS049 (-3.84), SS012 (-3.65), SS043 (-2.27), SS039 (-2.25), SS014 (-2.06), and SS09 (-1.98). SiO_2-rich rocks may have been responsible for the negative PC2 scores. The inputs of mica (muscovite) and quartz minerals may have contributed to the higher K_2O and SiO_2 concentrations, which consequently influenced the negative values of PC2. In the study area, these minerals are mostly ascribed to the existence of shales, micaceous shales and sandstones, conglomerates, sandstones, siltstones, claystones, mudstones, quartzites, mica schists, and other metamorphic rocks of the Aitutu, Wailuli, Viqueque, and Ainaro Formations, Lolotoi Complex, and Dilor Conglomerate, as well as exotic blocks of these rocks from the Lolotoi Complex, Aitutu Formation, and Wailuli Formation within the Bobonaro Complex.

Table 4. The first four principal components of the samples with eigenvalues greater than or near 1.0

	PC1	PC2	PC3		PC1	PC2	PC3		PC1	PC2	PC3
Eigenvalues	**4.97**	**2.02**	**1.36**	**Eigenvalues**	**4.97**	**2.02**	**1.36**	**Eigenvalues**	**4.97**	**2.02**	**1.36**
Explanation (%)	**49.74**	**20.23**	**13.61**	**Explanation (%)**	**49.74**	**20.23**	**13.61**	**Explanation (%)**	**49.74**	**20.23**	**13.61**
SS01	2.8094	-1.1265	0.3508	**SS019**	1.0377	1.6047	1.3011	**SS037**	0.1410	0.5790	1.1977
SS02	0.9505	-1.3944	-0.3555	**SS020**	1.8918	0.4021	1.0118	**SS038**	-0.6504	-0.8730	0.0325
SS03	-0.7047	0.9024	-0.5657	**SS021**	-0.2704	1.5562	1.8742	**SS039**	-1.3181	-2.2499	-0.4070
SS04	-4.2234	3.6410	-1.0284	**SS022**	2.5985	0.5487	-0.0845	**SS040**	3.1957	-0.4899	-1.3336
SS05	-0.5243	0.3881	-0.0213	**SS023**	3.5647	1.1403	0.3147	**SS041**	3.1437	0.1735	-1.1314
SS06	-4.0007	1.0310	-1.0535	**SS024**	-2.1377	1.1255	-0.5264	**SS042**	3.1120	0.0048	-1.3984
SS07	0.7688	0.1864	-0.3698	**SS025**	0.1876	1.5758	1.4588	**SS043**	0.6433	-2.2673	0.8850
SS08	0.2818	-0.1269	-0.4798	**SS026**	-1.7821	0.6782	-0.5172	**SS044**	2.3801	0.5704	-1.1502
SS09	-1.1991	-1.9787	1.8580	**SS027**	-0.7813	0.4200	0.0228	**SS045**	2.6404	2.3533	-0.4530
SS010	0.2185	-0.3535	-1.6808	**SS028**	-1.0743	0.2423	-0.4641	**SS046**	2.2837	0.2010	-1.1381
SS011	-1.4795	1.3840	-0.6523	**SS029**	-6.2286	1.1078	-2.1250	**SS047**	1.8602	0.2694	-1.5752
SS012	-1.9347	-3.6500	-0.6833	**SS030**	-2.8438	-0.1828	-1.0306	**SS048**	2.6183	0.4196	0.8197
SS013	-0.9795	-0.4875	2.2749	**SS031**	-1.3621	-0.1580	-0.9280	**SS049**	-1.7195	-3.8376	2.6119
SS014	-2.5533	-2.0583	-0.4066	**SS032**	-0.8008	-1.1856	-0.7950	**SS050**	3.2405	2.6371	2.5887
SS015	-5.0541	2.0570	2.4259	**SS033**	-0.4160	-0.0219	0.4749	**SS051**	2.1386	-0.1272	-0.6999
SS016	-1.7343	0.1991	1.2251	**SS034**	-0.2811	-0.8077	1.3272	**SS052**	2.3937	-0.3114	-0.7210
SS017	0.2471	-1.2933	-0.5948	**SS035**	1.6275	-0.0210	0.6776	**SS053**	0.6559	-1.1835	-0.5817
SS018	-0.0354	-1.2271	-0.3313	**SS036**	-0.5419	0.0145	0.5499				

 doi:10.20944/preprints202402.1202.v1

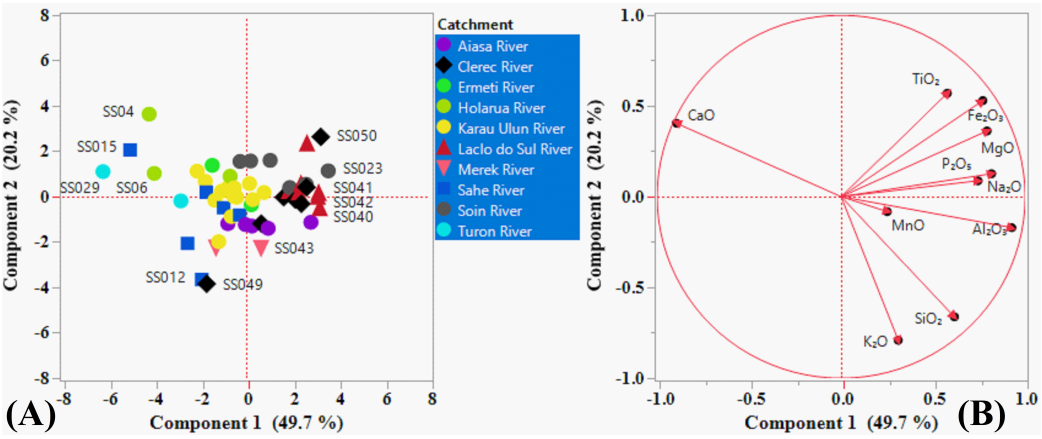

Figure 7. Component pattern plot of the first and second principal components for samples (A) and variables (B).

The third principal component had a strong positive loading for MnO (0.77), TiO_2 (0.42), K_2O (0.13), and Fe_2O_3 (0.11) and was strongly correlated with samples SS049 (2.61), SS050 (2.59), SS015 (2.43), SS013 (2.27), SS021 (1.87), and SS09 (1.86) (Tables 3 and 4, Figure 8). The elemental association of positive PC3 scores may be associated with contributions from manganese, siderite, pyrite, secondary Ti-bearing minerals and K-bearing minerals. In the study area, these minerals were ascribed to the presence of exotic blocks of garnet mica schists, mica schists, and quartzites within the Bobonaro Complex; sandstones and conglomerates rich in the Lolotoi Complex's metamorphic rock fragments of the Dilor Conglomerate; and altered siliciclastic sedimentary and carbonate rocks intercalated with shales due to metamorphic, silicification, and other alteration processes of the Wailuli and Aitutu Formations. Component 3 was also strongly associated in negative way with MgO (-0.32), Na_2O (-0.23), and Al_2O_3 (-0.20), and negative PC3 values were recorded for samples SS029 (-2.13), SS010 (-1.68), SS047 (-1.58), SS042 (-1.40), SS040 (-1.33), SS044 (-1.15), and SS046 (-1.14) (Tables 3 and 4, Figure 8). The occurrence of secondary mineral assemblages in low-grade metamorphic conditions, such as chlorite, albite, and epidote, could influence the negative PC3 values by contributing greater amounts of MgO, Na_2O, and Al_2O_3. These river sand samples were collected from shales, marls, sandstones, claystones, siltstones, conglomerates, and mudstone-rich formations affiliated with the Wailuli, Viqueque, Ainaro, and Suai Formations and the Bobonaro Complex.

The findings of the PCA were consistent with the results of the SiO_2/Al_2O_3 and K_2O/Na_2O ratios as well as those of the ICV.

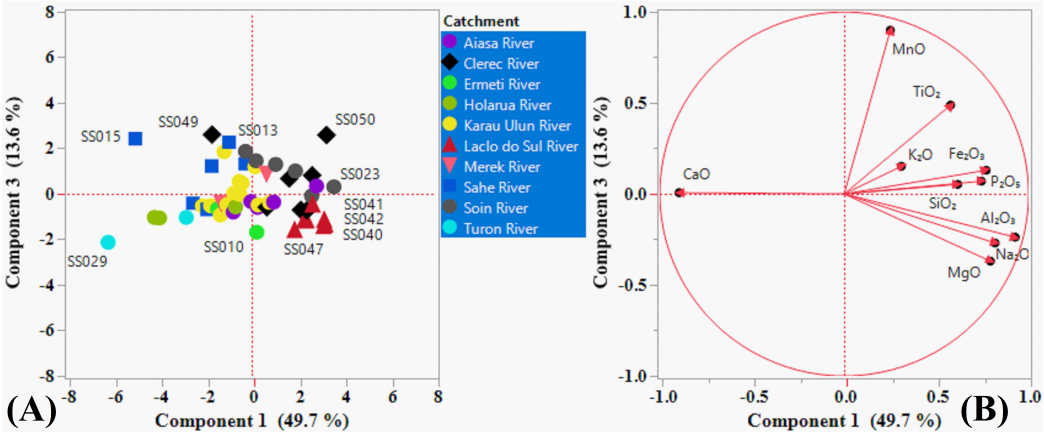

Figure 8. Component pattern plot of the first and third principal components for samples (A) and variables (B).

 doi:10.20944/preprints202402.1202.v1

6. Conclusion

The results of the bulk geochemical composition analysis of the river sand samples from the study area showed an abundance of CaO and a slight depletion in SiO_2 and Al_2O_3 concentrations, which were related to the major contributions from the calcareous cover sediments of the northern edge of the Australian continental shelf and from carbonate components that are integrated into sedimentary rocks in different proportions. Most of the catchment areas revealed a positive correlation between the SiO_2/Al_2O_3 ratios and most of the major elements, including the abundance of TiO_2, Fe_2O_3, MgO, and P_2O_5, and a positive relationship between high contents of TiO_2, Fe_2O_3, MnO, MgO, and P_2O_5. The average value of the K_2O/Na_2O ratio was less than 1, and the ICV was greater than 1, suggesting that clay, mica, and chlorite contents along with amphibole, pyroxene, biotite, ilmenite, hematite, sphene, rutile, garnet, and other minerals play a significant role in influencing the composition of the river sand samples. The enrichment of MnO may be explained by a significant contribution from manganese minerals and a lesser but considerable contribution from accessory, heavy, and mafic minerals (such as garnets, ilmenites, and pyroxenes). Calcareous sedimentary rocks such as calcilutites, calcareous shales, marls, and calcarenites are predominantly found in areas occupied by the Aitutu, Wailuli, and Viqueque Formations. Clay, mica, quartz, and other aluminosilicate contents were mainly sourced from shales, micaceous shales, micaceous sandstones, and their altered forms due to metamorphic processes, as well as claystones, siltstones, mudstones, sandstones, conglomerates, and quaternary sediments, which are found in areas covered by the Wailuli, Viqueque, Ainaro, and Suai Formations, as well as the Bobonaro Complex and Dilor Conglomerate. In contrast, mafic sources containing heavy and accessory minerals (such as amphiboles, pyroxenes, biotites, ilmenites, hematites, sphenes, rutiles, and garnets) were related to the presence of basic igneous, metamorphic, conglomerate, shales, and mudstones. These rocks are mostly found in regions encompassed by the Wailuli Formation, Bobonaro Complex, Dilor Conglomerate, and Ainaro Formation as well as near the contact between the Lolotoi Complex and the Wailuli Formation. High concentrations of MnO, SiO_2, and K_2O were also recorded at sampling sites covered by carbonate rocks intercalated with shales of the Wailuli and Aitutu Formations (SS049, SS014, and SS015). In the drainage basins from these sampling locations, a positive correlation was identified between SiO_2, CaO, and K_2O, and CaO was positively associated with MnO; however, CaO, MnO, and TiO_2 were positively correlated. These results were related to the occurrence of quartz and secondary K-bearing minerals and Ti-bearing minerals associated with calcium carbonate and manganese minerals in carbonate rocks that have undergone silicification and other alteration processes.

These findings were also supported by the PCA results, which showed that the first and second principal components were correlated with the origin and composition of the underlying lithologies and that PC3 could possibly reveal the presence and distribution of alteration minerals related to metamorphism and hydrothermalism. The first principal component was associated with variations in Ca-poor and Ca-rich rocks, with positive scores indicating significant contributions from clay minerals and negative scores indicating a notable input from carbonate components. PC2 may capture the variations associated with compositional differences between the SiO_2-rich and SiO_2-poor rocks. Positive PC2 scores suggested notable inputs from amphibole, pyroxene, biotite, ilmenite, rutile, and garnet minerals. Mica (muscovites) and quartz minerals may have contributed significantly to negative PC2 values. PC3 explained the occurrence and distribution of altered minerals related to metamorphism and hydrothermalism. Positive values indicated the possibility of contributions from Mn, siderite, pyrite, secondary Ti-bearing minerals, and secondary K-bearing minerals. The negative PC3 scores could be related to inputs from low-grade metamorphic mineral assemblages, such as chlorite, albite, and epidote.

This study proved that river sand geochemical mapping is a valuable tool for lithological mapping in areas with limited geological information because of limited accessibility and dense vegetation coverage, as well as deformed, weathered, and erosion-covered geological materials.

 doi:10.20944/preprints202402.1202.v1

Author Contributions: Vital Vilanova: Conceptualization, Methodology, Validation, Investigation, Formal Analysis, Writing—original draft. Tomoyuki Ohtani: Validation, Supervision, Visualization, Writing—review and editing. Satoru Kojima: Validation, Supervision, Visualization, Writing—review and editing. Kazuma Yatabe: Formal analysis. Nene Cristovão and Aniceta Araujo: Investigation, Formal Analysis. All authors have read and agreed to the published version of the paper.

Funding: This research and the APC were funded by the Japan International Cooperation Agency (JICA) Development Studies Program, Human Resources Development in Science and Technology Innovation and the Earth Science Laboratory, Faculty of Engineering, Gifu University.

Acknowledgments: This study was financially supported by the Japan International Cooperation Agency (JICA) Development Studies Program and Human Resources Development in Science and Technology Innovation. We are grateful to Professor Nagayoshi Katsuta and Mr. Matsuki of Gifu University for permitting us to use the laboratory to prepare glass bead samples. We also thank the staff of the Ministry of Petroleum and Mineral Resources, particularly the Institute of Petroleum and Geology and the National Petroleum and Minerals Authority, Dili, Timor-Leste, for authorizing the shipment of samples from Timor-Leste to Japan. We express our gratitude to the Nagoya University Museum, JICA, and Faculty of Engineering of the Gifu University staff members, Prof. Dr. Koshi Yamamoto, Prof. Dr. Koichi Shimakawa, Mr. Atsushi Takahashi, Ms. Mieko Araki, Ms. Yukiko Eguchi, and Ms. Midori Iinuma.

Conflicts of Interest: The authors declare that they have no conflicts of financial or non-financial interests that could impact the subject matter or reported research results in this paper.

Abbreviations

The following abbreviations are used in this paper:

PCA	Principal component analysis
PC1	Principal component 1
PC2	Principal component 2
PC3	Principal component 3
ICV	Index of compositional variability
XRF	X-ray fluorescence
UCC	Upper continental crust
PAAS	Post-Archean Australian Shale
Mn	Manganese
K-bearing minerals	Potassium-bearing minerals
Ti-bearing minerals	Titanium-bearing minerals
JMP	Jump, statistical analysis software developed by JMP
ArcGIS	Aeronautical Reconnaissance Coverage Geographic Information System
JICA	Japan International Cooperation Agency

References

1. Audley-Charles, M. G. The Geology of Portuguese Timor. *Memoirs of the Geological Society of London* **1968**, *4*, 1–75.
2. Audley-Charles, M. G. Tectonic Post-Collision Processes in Timor. *The Geological Society of London, Special Publication* **2011**, *355*, 241–266. https://doi.org/10.1144/SP355.12.
3. Audley-Charles, M. G., Carter, D. J., & Barber, A. J. Stratigraphic Basis for Tectonic Interpretation of the Outer Banda Arc, Eastern Indonesia. *Proceeding Indonesian Petroleum Association*, Indonesia, Third Annual Convention, **June 1974**, 25–44.
4. Audley-Charles, M. G., & Carter, D. J. Tectonic Post-Collision Processes in Timor. *Palaeogeographical Significance of Some Aspect of Palaeogene and Early Neogene Stratigraphy and Tectonics of the Timor Sea Region* **1972**, *11*, 247–264.
5. Bachri, S., & Situmorang, R. L. Peta Geologi Lembar Dili, Timor Timur, Skala 1: 250.000. *Pusat Penelitian dan Pengembangan Geologi*, 1994.
6. Barber, A. J., & Audley-Charles, M. G. The Significance of the Metamorphic Rocks of Timor in the Development of the Banda Arc, Eastern Indonesia. *Tectonophysics* **1976**, *30*, 119–128.

7. Boger, S. D., Spelbrink, L. G., Lee, R. I., Sandiford, M., Maas, R., & Woodhead, J. D. Isotopic (U-Pb, Nd) and Geochemical Constraints on the Origins of the Aileu and Gondwana Sequences of Timor. *Journal of Asian Earth Sciences* **2017**, *134*, 330–351. https://doi.org/10.1016/j.jseaes.2016.11.026.
8. Charlton, T. R. Stratigraphic Correlation Across an Arc-Continent Collision Zone: Timor and the Australian Northwest Shelf. *Australian Journal of Earth Sciences* **1989**, *36*, 263–274.
9. Charlton, T. R. Post-Collision Extension in Arc-Continent Collision Zones, Eastern Indonesia. *Geology* **1991**, *19(1)*, 28–31. https://doi.org/10.1130/0091-7613(1991)019<0028:PEIACC>2.3.CO;2.
10. Charlton, T. R. The Structural Setting and Tectonic Significance of the Lolotoi, Laclubar and Aileu Metamorphic Massifs, East Timor. *Journal of Asian Earth Sciences* **2002**, *20*, 851–865. www.elsevier.com/locate/jseaes.
11. Charlton, T. R., Barber, A. J., Harris, R. A., Barkham, S. T., Bird, P. R., Archbold, N. W., Morris, N. J., Nicoll, R. S., Owen, H. G., Owens, R. M., Sorauf, J. E., Taylor, P. D., Webster, G. D., & Whittaker, J. E. The Permian of Timor: Stratigraphy, Palaeontology and Palaeogeography. *Journal of Asian Earth Sciences* **2002**, *20*, 719–774. www.elsevier.com/locate/jseaes.
12. Charlton, T. R., Barber, A. J., McGowan, A. J., Nicoll, R. S., Roniewicz, E., Cook, S. E., Barkham, S. T., & Bird, P. R. The Triassic of Timor: Lithostratigraphy, Chronostratigraphy and Palaeogeography. *Journal of Asian Earth Sciences* **2009**, *36(4-5*, 341–363. https://doi.org/10.1016/j.jseaes.2009.06.004.
13. Ely, K. S., Sandiford, M., Hawke, M. L., Phillips, D., Quigley, M., & Reis, J. E. dos. Evolution of Ataúro Island: Temporal constraints on subduction processes beneath the Wetar zone, Banda Arc. *Journal of Asian Earth Sciences* **2011**, *41(6)*, 477–493. https://doi.org/10.1016/j.jseaes.2011.01.019.
14. Haig, D. W. Palaeobathymetric Gradients Across Timor During 5.7 - 3.3 Ma (Latest Miocene-Pliocene) and Implications for Collision Uplift. *Palaeogeography, Palaeoclimatology, Palaeoecology* **2012**, *331-332*, 50–59. https://doi.org/10.1016/j.palaeo.2012.02.032.
15. Haig, D. W., McCartain, E., Barber, L., & Backhouse, J. Triassic - Lower Jurassic Foraminiferal Indices for Bahaman - Type Carbonate - Bank Limestones, Cablac Mountain, East Timor. *Journal of Foraminiferal Research* **2007**, *37(3)*, 248–264.
16. Haig, D. W., McCartain, E. W., Keep, M., & Barber, L. Re-evaluation of the Cablac Limestone at Its Type Area, East Timor: Revision of the Miocene Stratigraphy of Timor. *Journal of Asian Earth Sciences* **2008**, *33(5-6)*, 366–378. https://doi.org/10.1016/j.jseaes.2008.03.002.
17. Haig, D. W., Mossadegh, Z. K., Parker, J. H., & Keep, M. Middle Eocene neritic limestone in the type locality of the volcanic Barique Formation, Timor-Leste: Microfacies, age and tectonostratigraphic affinities. *Journal of Asian Earth Sciences* **2019**, *X*, 1. https://doi.org/10.1016/j.jaesx.2018.100003.
18. Harris, R. A. Rise and Fall of the Eastern Great Indonesian Arc Recorded by the Assembly, Dispersion and Accretion of the Banda Terrane, Timor. *Gondwana Research* **2006**, *10(3-4)*, 207–231. https://doi.org/10.1016/j.gr.2006.05.010.
19. Harris, R. A. The Nature of the Banda Arc - Continent Collision in the Timor Region. *Arc-Continent Collision, Frontiers in Earth Sciences* **2011**, *4*, 163–211. https://doi.org/10.1007/978-3-540-88558-0_7.
20. Keep, M., & Haig, D. W. Deformation and Exhumation in Timor: Distinct Stages of a Young Orogeny. *Tectonophysics* **2009**, *483(1-2)*, 93–111. https://doi.org/10.1016/j.tecto.2009.11.018.
21. Leme, J. C. A. Breve Ensaio Sobre a Geologia da Província de Timor. *Junta de Investigações do Ultramar, Geólogo da Missão de Estudos Agronómicos do Ultramar* **1968**, *1*, 106–161.
22. Lisboa, J. V. V., Silva, T. P., De Oliveira D. P. S, & Carvalho, J. F. Mineralogical and Geochemistry Characteristics of the Bobonaro Melange of Western East Timor: Provenance Implications. *Comunicações Geológicas* **2020**, *106(I)*, 35–49. https://www.lneg.pt/wp-content/uploads/2020/05/Volume_106.pdf.
23. Park, S.-I., Kwon, S., & Kim, S. W. Evidence for the Jurassic Arc Volcanism of the Lolotoi complex, Timor: Tectonic Implications. *Journal of Asian Earth Sciences* **2014**, *95*, 254–265. https://doi.org/10.1016/j.jseaes.2014.05.007.
24. Partoyo, E., Hermanto, B., & Bachri, S. Peta Geologi Lembar Baucau, Timor Timur, Skala 1: 250.000. *Pusat Penelitian dan Pengembangan Geologi.*, 1995.
25. Standley, C. E., & Harris, R. Tectonic Evolution of Forearc Nappes of the Active Banda Arc - Continent Collision: Origin, Age, Metamorphic History and Structure of the Lolotoi Complex, East Timor. *Tectonophysics* **2009**, *479(1-2)*, 66–94. https://doi.org/10.1016/j.tecto.2009.01.034.

 doi:10.20944/preprints202402.1202.v1

26. Wittouck, S. F. Exploration of Portuguese Timor. *Report of Allied Mining Corporation to Asia Investment Company, Limited* **1937**.
27. Audley-Charles, M. G. The Geology of Portuguese Timor. Doctor Thesis, University of London, London–England, March 1965.
28. Barber, A. J., Audley-Charles, M. G., & Carter, D. J. Thrust Tectonics in Timor. *Journal of the Geological Society of Australia* **1977**, *24(1-2)*, 51–62. https://doi.org/10.1080/00167617708728966.
29. Carter, D. J., Audley-Charles, M. G., & Barber, A. J. Stratigraphical Analysis of Island Arc - Continental Margin Collision in Eastern Indonesia. *The Journal of Geological Society of London* **1976**, *132(2)*, 179–198.
30. Grady, A. E., & Berry, R. F. Some Palaeozoic - Mesozoic Stratigraphic - Structural Relationships in East Timor and Their Significance in the Tectonics of Timor. *Journal of the Geological Society of Australia* **1977**, *24(3-4)*, 203–214. https://doi.org/10.1080/00167617708728981.
31. Harris, R. A., & Long, T. The Timor Ophiolite, Indonesia: Model or Myth?. *Geological Society of America* **2000**, *349*, 321–330.
32. Bineli, M. T. N., Onana, V. L., Noa Tang, S. D., Bikoy, Y. R., & Ekodeck, G. E. Mineralogy and geochemistry of sands of the lower course of the Sanaga River, Cameroon: implications for weathering, provenance, and tectonic setting. *Acta Geochimica* **2021**, *40(3)*, 348–365. https://doi.org/10.1007/s11631-020-00437-z.
33. Brundin, N. H., & Nairis, B. Alternative Sample Types in Regional Geochemical Prospecting. *Journal of Geochemical Exploration* **1972**, *1*, 7–46.
34. Franzinelli, E., & Potter, P. E. Petrology, Chemistry, and Texture of Modern River Sands, Amazon River System. *Journal of Geology* **1983**, *91*, 23–39. http://www.journals.uchicago.edu/t-and-c.
35. Liyouck, P. R., Ngueutchoua, G., Armstrong-Altrin, J. S., Sonfack, A. N., Kontchipe Ngagoum, Y. S., Ekoa Bessa, A. Z., Ambassa Bela, V., Tsanga, D. A., & Wouatong, A. S. L. Petrography and geochemistry of the Sanaga river sediments, central Cameroon: Constraints on weathering, provenance, and tectonic setting. *Journal of African Earth Sciences, 199, 104840* **2023**, *199 (104840)*. https://doi.org/10.1016/j.jafrearsci.2023.104840.
36. Nesbitt, H. W., & Young, G. M. Petrogenesis of sediments in the absence of chemical weathering: Effects of abrasion and sorting on bulk composition and mineralogy. *Sedimentology* **1996**, *43(2)*, 341–358. https://doi.org/10.1046/j.1365-3091.1996.d01-12.x.
37. Nurmi, P. A., & Isohanni, M. Rock, Till, and Stream Sediment Geochemistry in the Search for Porphyry-Type Mo-Cu-Au Deposit in the Proterozoic Rautio Batholith, Western Finland. *Journal of Geochemical Exploration* **1984**, *20*, 209–228.
38. Ortiz, E., & Roser, B. P. Geochemistry of Stream Sediments from the Hino River, SW Japan: Source Rock Signatures, Downstream Compositional Variations, and Influence of Sorting and Weathering. *Earth Science (Chikyu Kagaku)* **2006a**, *60*, 131–146.
39. Ortiz, E., & Roser, B. P. Major and trace element provenance signatures in stream sediments from the Kando River, San'in district, southwest Japan. *Island Arc* **2006b**, *15(2)*, 223–238. https://doi.org/10.1111/j.1440-1738.2006.00523.x.
40. Rahman, M. A., Das, S. C., Pownceby, M. I., Tardio, J., Alam, M. S., & Zaman, M. N. Geochemistry of Recent Brahmaputra River Sediments: Provenance, Tectonics, Source Area Weathering and Depositional Environment. *Minerals* **2020**, *10(9)*, 1–30. https://doi.org/10.3390/min10090813.
41. Ranasinghe, P. N., Fernando, G. W. A. R., Dissanayake, C. B., & Rupasinghe, M. S. Stream Sediment Geochemistry of the Upper Mahaweli River Basin of Sri Lanka-Geological and Environmental Significance. *Journal of Geochemical Exploration, 99(1–3), 1–28* **2008**, *99(1-3)*, 1–28. https://doi.org/10.1016/j.gexplo.2008.02.001.
42. Yamamoto, K., Tanaka, T., Minami, M., Mimura, K., Asahara, Y., Yoshida, H., Yogo, S., Takeuchi, M., & Inayoshi, M. Geochemical Mapping in Aichi Prefecture, Japan: Its Significance as a Useful Dataset for Geological Mapping. *Applied Geochemistry* **2007**, *22(2)*, 306–319. https://doi.org/10.1016/j.apgeochem.2006.09.011.
43. Young, S. M., Pitawala, A., & Ishiga, H. Geochemical Characteristics of Stream Sediments, Sediment Fractions, Soils, and Basement Rocks from the Mahaweli River and Its Catchment, Sri Lanka. *Chemie Der Erde* **2013**, *73(3)*, 357–371. https://doi.org/10.1016/j.chemer.2012.09.003.

 doi:10.20944/preprints202402.1202.v1

44. Pan, T., Zuo, R., & Wang, Z. Geological Mapping via Convolutional Neural Network Based on Remote Sensing and Geochemical Survey Data in Vegetation Coverage Areas. *IEEE Journal of Selected Topics in Applied Earth Observations and Remote Sensing* **2023**, *16*, 3485–3494. https://doi.org/10.1109/JSTARS.2023.3260584.
45. Audley-Charles, M. G. Geometrical Problems and Implications of Large-Scale Over-Thrusting in the Banda Arc - Australian Margin Collision Zone. *The Geological Society of London* **1981**, 407–416.
46. Audley-Charles, M. G. Rates of Neogene and Quaternary Tectonic Movements in the Southern Banda Arc Based on Micropalaeontology. *Journal of the Geological Society, London* **1986**, *143*, 161–175.
47. Audley-Charles, M. G. Ocean Trench Blocked and Obliterated by Banda Forearc Collision with Australian Proximal Continental Slope. *Tectonophysics* **2004**, *389(1-2)*, 65–79. https://doi.org/10.1016/j.tecto.2004.07.048.
48. Barber, A. J. Structural Interpretations of the Island of Timor, Eastern Indonesia. *The Geology and Tectonics of Eastern Indonesia, Geological Research and Development Centre* **1981**, *2*, 183–197.
49. Berry, R. F., & Grady, A. E. Deformation and Metamorphism of the Aileu Formation, North Coast, East Timor and Its Tectonic Significance. *Journal of Structural Geology* **1981**, *3(2)*, 143–167.
50. Berry, R. F., & Jenner, G. A. Basalt Geochemistry as a Test of the Tectonic Models of Timor. *Journal of Geological Society of London* **1982**, *139*, 593–604.
51. Charlton, T. R. Tertiary Evolution of the Eastern Indonesia Collision Complex. *Journal of Asian Earth Sciences* **2000**, *18*, 603–631
52. Duffy, B., Quigley, M., Harris, R., & Ring, U. Arc - Parallel Extrusion of the Timor Sector of the Banda Arc - Continent Collision. *Tectonics* **2013**, *32(3)*, 641–660. https://doi.org/10.1002/tect.20048.
53. Duffy, B., Kalansky, J., Bassett, K., Harris, R., Quigley, M., van Hinsbergen, D. J. J., Strachan, L. J., & Rosenthal, Y. Mélange Versus Forearc Contributions to Sedimentation and Uplift, During Rapid Denudation of a Young Banda Forearc-Continent Collisional Belt. *The Journal of Asian Earth Sciences* **2017**, *138*, 186–210. https://doi.org/10.1016/j.jseaes.2017.02.008.
54. Haig, D. W., Rigaud, S., McCartain, E., Martini, R., Barros, I. S., Brisbout, L., Soares, J., & Nano, J. Upper Triassic carbonate-platform facies, Timor-Leste: Foraminiferal indices and regional tectonostratigraphic association. *Palaeogeography, Palaeoclimatology, Palaeoecology* **2021**, *570*, 241–266. https://doi.org/10.1016/j.palaeo.2021.110362.
55. Harris, R. A., Kaiser, J., Hurford, A., & Carter, A. Thermal History of Australian Passive Margin Cover Sequences Accreted to Timor During Late Neogene Arc - Continent Collision, Indonesia. *Journal of Asian Earth Sciences* **2000**, *18*, 47–69.
56. Harris, R. A., Vorkink, M. W., Prasetyadi, C., Zobell, E., Roosmawati, N., & Apthorpe, M. Transition from Subduction to Arc-Continent Collision: Geologic and Neotectonic Evolution of Savu Island, Indonesia. *Geosphere* **2009**, *5(3)*, 152–171. https://doi.org/10.1130/GES00209.1.
57. Kaneko, Y., Maruyama, S., Kadarusman, A., Ota, T., Ishikawa, M., Tsujimori, T., Ishikawa, A., & Okamoto, K. On-Going Orogeny in The Outer-Arc of the Timor-Tanimbar Region, Eastern Indonesia. *Gondwana Research* **2007**, *11(1-2)*, 218–233. https://doi.org/10.1016/j.gr.2006.04.013.
58. Price, N. J., & Audley-Charles, M. G. Tectonic Collision Processes After Plate Rupture. *Tectonophysics* **1987**, *140*, 121–129.
59. Tate, G. W., McQuarrie, N., Van Hinsbergen, D. J. J., Bakker, R. R., Harris, R., Willett, S., Reiners, P. W., Fellin, M. G., Ganerød, M., & Zachariasse, W. J. Resolving Spatial Heterogeneities in Exhumation and Surface Uplift in Timor-Leste: Constraints on Deformation Processes in Young Orogens. *Tectonics* **2014**, *33(6)*, 1089–1112. https://doi.org/10.1002/2013TC003436.
60. Tate, G. W., McQuarrie, N., Van Hinsbergen, D. J. J., Bakker, R. R., Harris, R., & Jiang, H. Australia Going Down Under: Quantifying Continental Subduction During Arc-Continent Accretion in Timor-Leste. *Geosphere* **2015**, *11(6)*, 1860–1883. https://doi.org/10.1130/GES01144.1.
61. Tate, G. W., McQuarrie, N., Tiranda, H., van Hinsbergen, D. J. J., Harris, R., Zachariasse, W. J., Fellin, M. G., Reiners, P. W., & Willett, S. D. Reconciling Regional Continuity with Local Variability in Structure, Uplift and Exhumation of the Timor Orogen. *Gondwana Research* **2017**, *49*, 364–386. https://doi.org/10.1016/j.gr.2017.06.008.
62. Audley-Charles, M. G., & Harris, R. Allochthonous Terranes of the Southwest Pacific and Indonesia. *Philosophical Transactions of the Royal Society of London* **1990**, *331(1620)*, 571–587.

63. Keep, M., Barber, L., & Haig, D. Deformation of the Cablac Mountain Range, East Timor: an Overthrust Stack Derived from an Australian Continental Terrace. *Journal of Asian Earth Sciences* **2009**, *35(2)*, 150–166. https://doi.org/10.1016/j.jseaes.2009.02.001.
64. Audley-Charles, M. G. Paleoenvironmental Significance of Chert in the Franciscan Formation of Western California: Discussion Concerning the Significance of Chert in Timor. *Geological Society of America Bulletin* **1973**, *84(2)*, 363–368.
65. Barber, A. J., Tjokrosapoetro, S., & Charlton, T. R. Mud Volcanoes, Shale Diapirs, Wrench Faults, and Melanges in Accretionary Complexes, Eastern Indonesia. *The American Association of Petroleum Geologists* **1986**, *70(11)*, 1729–1741.
66. Charlton, T. R., & Wall, D. New Biostratigraphic Results from the Kolbano Area, Southern West Timor: Implications for the Mesozoic-Tertiary Stratigraphy of Timor. *ournal of Southeast Asian Earth Sciences* **1994**, *9(2)*, 113–122.
67. Earle, M. The Metamorphic Rocks of Boi, Timor, Eastern Indonesia. *The Geology and Tectonics of Eastern Indonesia, Geological Research and Development Centre* **1981**, *2*, 239–251. https://www.researchgate.net/publication/285976880.
68. Haig, D. W., McCartain, E., Mory, A. J., Borges, G., Davydov, V. I., Dixon, M., Ernst, A., Groflin, S., Håkansson, E., Keep, M., Santos, Z. Dos, Shi, G. R., & Soares, J. Postglacial Early Permian (late Sakmarian-early Artinskian) shallow-marine carbonate deposition along a 2000km transect from Timor to west Australia. *Palaeogeography, Palaeoclimatology, Palaeoecology* **2014**, *409*, 180–204. https://doi.org/10.1016/j.palaeo.2014.05.009.
69. Haig, D. W., & McCartain, E. Carbonate Pelagites in the Post-Gondwana Succession (Cretaceous - Neogene) of East Timor. *Australian Journal of Earth Sciences* **2007**, *54(6)*, 875–897. https://doi.org/10.1080/08120090701392739.
70. Haig, D. W., & McCartain, E. Triassic Organic - Cemented Siliceous Agglutinated Foraminifera from Timor Leste: Conservative Development in Shallow - Marine Environments. *Journal of Foraminiferal Research* **2010**, *40(4)*, 366–392.
71. Harris, R. A. Temporal Distribution of Strain in the Active Banda Orogen: a Reconciliation of Rival Hypotheses. *Journal of Southeast Asian Earth Sciences* **1991**, *6(3/4)*, 373—386.
72. Harris, R. A., Sawyer, R. K., & Audley-Charles, M. G. Collisional Melange Development: Geologic Associations of Active Melange-Forming Processes with Exhumed Melange Facies in the Western Banda Orogen, Indonesia. *Tectonics* **1998**, *17(3)*, 458–479.
73. Kenyon, C. S. Stratigraphy and Sedimentology of the Late Miocene to Quaternary Deposits of Timor. Doctor Thesis, University of London, London–England, May 1974.
74. Hale, M., & Plant, J. A. Introduction: The Foundation of Modern Drainage Geochemistry. In *Handbook of Exploration Geochemistry: Drainage Geochemistry*; Govett, G. J. S, Elsevier Science B.V; Amsterdam, Netherlands, 1994; pp. 3–9.
75. Darnley, A. G., Bjorklund, A., Bolviken, B., Gustavsson, N., Koval, P. V., Plant, J. A., Steenfelt, A., Tauchid, M., Xuejing, X., Garrett, R. G., & Hall, G. E. M. A Global Geochemical Reference Network & Field Methods for Regional Surveys. In *A Global Geochemical Database for Environmental and Resource Management: Recommendations for International Geochemical Mapping*; United Nations Educational, Scientific and Cultural Organization (UNESCO); Publishing House: Paris, France, 1995; pp. 37–53.
76. Tanaka, T., Kawabe, I., Yamamoto, K., Iwamori, H., Hirahara, Y., Mimura, K., Asahara, Y., Ito, T., Yonezawa, C., Dragusanu, C., Kanda, S., Shimizu, O., Hayashi, M., Miura, N., Aoki, H., Ohta, A., Togami, K., Toriumi, T., Matsumura, Y., Sakakibara, T., Tanimizu, M., Mizutani, Y., Miyanaga, N., Murayama, M., & Ohmori, F. Distributions of Elements in Stream Sediments in and around Seto City, Aichi Prefecture: An Attempt to a Geoenvironmental Assessment by Geochemical Mapping. *Geochemistry* **1995**, *29*, 113–125.
77. Fletcher, W. K. Stream Sediment Geochemistry in Today´s Exploration World. Proceedings of Exploration 97: Fourth Decennial International Conference on Mineral Exploration. In A. G. Gubins (Ed.), 1997, pp 249-–260.
78. Ohta, A., Imai, N., Terashima, S., & Tachibana, Y. Application of Multi-Element Statistical Analysis for Regional Geochemical Mapping in Central Japan. *Applied Geochemistry* **2005**, *20(5)*, 1017–1037. https://doi.org/10.1016/j.apgeochem.2004.12.005.
79. Yamamoto, K., & Morishita, T. Preparation of Standard Composites for the Trace Elements Analysis by X-Ray Fluorescence. *Geological Society of Japan* **1997**, *103(11)*, 1037–1045.

80. Rudnick, R. L., & Gao, S. Composition of the Continental Crust. In *Treatise on Geochemistry*; Holland, H. D., & Turekian, K. K.; USA, 2003; Volume I, pp. 1–64. https://doi.org/10.1016/B0-08-043751-6/03016-4.
81. Taylor, S. R., & McLennan, S. M. *The Continental Crust: Its Composition and Evolution*; Blackwell Scientific Publications, Oxford, UK, 1985.
82. Demšar, U., Harris, P., Brunsdon, C., Fotheringham, A. S., & McLoone, S. Principal Component Analysis on Spatial Data: An Overview. *Annals of the Association of American Geographers* **2013**, *103(1)*, 106–128. https://doi.org/10.1080/00045608.2012.689236.
83. Reimann, C., Filzmoser, P., Garrett, R. G., & Dutter, R. Principal Component Analysis (PCA) and Factor Analysis (FA). In *Statistical Data Analysis Explained: Applied Environmental Statistics with R*; John Wiley & Sons, Ltd.; West Sussex, England, 2008; pp. 211–232.
84. Biswas, P. K., Alam, M. S., Hasan, A. S. M. M., Ahmed, S. S., & Zaman, M. N. Geochemical signatures of recent bar deposits in the Tista river, Bangladesh: Implications to provenance, paleoweathering and tectonics. *Journal of Nepal Geological Society* **2020**, *60*, 1–20. https://doi.org/10.3126/jngs.v60i0.31272.
85. He, M., Zheng, H., Clift, P. D., Tada, R., Wu, W., & Luo, C. Geochemistry of fine-grained sediments in the Yangtze River and the implications for provenance and chemical weathering in East Asia. *Progress in Earth and Planetary Science* **2015**, *2(1)*. https://doi.org/10.1186/s40645-015-0061-6.
86. Hossain, H. M. Z. Major, trace, and REE geochemistry of the Meghna River sediments, Bangladesh: Constraints on weathering and provenance. *Geological Journal* **2020**, *55(5)*, 3321–3343. https://doi.org/10.1002/gj.3595.
87. Kimeli, A., Ocholla, O., Okello, J., Koedam, N., Westphal, H., & Kairo, J. Geochemical and petrographic characteristics of sediments along the transboundary (Kenya-Tanzania) Umba River as indicators of provenance and weathering. *Open Geosciences* **2021**, *13(1)*, 1064–1083. https://doi.org/10.1515/geo-2020-0275.
88. Kontchipe, Y. S. N., Sopie, F. T., Ngueutchoua, G., Sonfack, A. N., Nkouathio, D. G., Tchatchueng, R., Nguemo, G. R. K., & Njanko, T. Mineralogy and Geochemistry Study of the Nyong River Sediments, SW Cameroon: Implications for Provenance, Weathering, and Tectonic Setting. *Arabian Journal of Geosciences* **2021**, *14(1018)*, 1–26. https://doi.org/10.1007/s12517-021-07145-9/Published.
89. Sonfack, A. N., Ngueutchoua, G., Kontchipe, Y. S. N., Sopie, F. T., Nkouathio, D. G., Wouatong, A. S. L., Tchatchueng, R., Kenfack Nguemo, G. R., & Njanko, T. Mineralogical and Geochemical Signatures of Surface Stream Sediments from Dibamba River Basin, SW Cameroon: Implications for Provenance, Weathering, and Tectonic Setting. *Journal of African Earth Sciences* **2011**, *181*, 1–26. https://doi.org/10.1016/j.jafrearsci.2021.104251.
90. Cox, R., Lowe, D. R., & Cullers, R. L. The Influence of Sediment Recycling and Basement Composition on Evolution of Mudrock Chemistry in the Southwestern United States. *Geochimica et Cosmochimica Acta* **1995**, *59(14)*, 2919–2940. https://doi.org/10.1016/0016-7037(95)00185-9.
91. Zuffa, G. G. Unravelling Hinterland and Offshore Palaeogeography from Deep-water Arenites. *Marine Clastic Seimentology* **1987**, 39–61.
92. McLennan, S. M., Hemming, S., McDaniel, D. K., & Hanson, G. N. Geochemical Approaches to Sedimentation, Provenance, and Tectonics. *Geological Society of America* **1993**, *284*, 21–40. https://doi.org/10.1130/SPE284-p21.
93. Herron, M. M. Geochemical Classification of Terrigenous Sands and Shales from Core or Log Data. *Sedimentary Petrology* **1988**, *58(5)*, 820–829. https://doi.org/10.1306/212f8e77-2b24-11d7-8648000102c1865d.
94. Pettijohn, F. J., Potter, P. E., & Siever, R. *Sand and Sandstone*; Springer - Verlag; New York, USA, January 1972; pp. 1–618. https://doi.org/10.1007/978-1-4615-9974-6.
95. Roser, B. P., Cooper, R. A., Nathan, S., & Tulloch, A. J. Reconnaissance Sandstone Geochemistry, Provenance, and Tectonic Setting of the Lower Paleozoic Terranes of the West Coast and Nelson, New Zealand. *New Zealand Journal of Geology and Geophysics* **1996**, *39(1)*, 1–16. https://doi.org/10.1080/00288306.1996.9514690.
96. Armstrong-Altrin, J. S., Nagarajan, R., Madhavaraju, J., Rosalez-Hoz, L., Lee, Y. Il, Balaram, V., Cruz-Martínez, A., & Avila-Ramírez, G. Geochemistry of the Jurassic and Upper Cretaceous Shales from the Molango Region, Hidalgo, Eastern Mexico: Implications for Source-Area Weathering, Provenance, and Tectonic Setting. *Comptes Rendus - Geoscience* **2013**, *345(4)*, 185–202. https://doi.org/10.1016/j.crte.2013.03.004.

 doi:10.20944/preprints202402.1202.v1

97. Armstrong-Altrin, J. S., Botello, A. V., Villanueva, S. F., & Soto, L. A. Geochemistry of Surface Sediments from the Northwestern Gulf of Mexico: Implications for Provenance and Heavy Metal Contamination. *Geological Quarterly* **2019**, *63(3)*, 522–538. https://doi.org/10.7306/gq.1484.
98. Kassi, A. M., Grigsby, J. D., Khan, A. S., & Kasi, A. K. Sandstone Petrology and Geochemistry of the Oligocene-Early Miocene Panjgur Formation, Makran Accretionary Wedge, Southwest Pakistan: Implications for Provenance, Weathering and Tectonic Setting. *Journal of Asian Earth Sciences* **2015**, *105*, 192–207. https://doi.org/10.1016/j.jseaes.2015.03.021.
99. Armstrong-Altrin, J. S. Detrital zircon U–Pb geochronology and geochemistry of the Riachuelos and Palma Sola beach sediments, Veracruz State, Gulf of Mexico: a new insight on palaeoenvironment. *Journal of Palaeogeography* **2020**, *9(1)*. https://doi.org/10.1186/s42501-020-00075-9.